Formation integrity evaluation for geosequestration of CO2 in depleted petroleum reservoirs under cyclic stress conditions.

AMINAHO, E.N., HOSSAIN, M., FAISAL, N.H. and SANAEE, R.

2024

ABSTRACT

The geological storage of carbon dioxide (CO_2), also referred to as CO_2 geosequestration, represents one of the most promising options for reducing greenhouse gases in the atmosphere. However, most of the time, CO_2 is captured with small amounts of other industrial gases such as sulphur dioxide (SO_2) and hydrogen sulphide (H_2S), which might be compressed together and stored in depleted petroleum reservoirs or aquifers. Moreover, during CO_2 geosequestration in reservoirs, pressure variations during injection could force some amount of CO_2 (with or without other acid gas impurities) into the caprock; thereby, altering the petrophysical, geochemical, and geomechanical properties of the caprock. Thus, the brittleness index of the reservoir and caprock might be impacted during CO_2 geosequestration due to the chemical reactions between the rock minerals and the formation fluid. Furthermore, to meet the world net-zero carbon target, the promotion of CO_2 utilization is paramount. This could be possible by developing an effective technology for cyclic CO_2 geosequestration (with or without gas impurities). Therefore, studies on the co-injection of CO_2 with other acid gases from industrial emissions, their withdrawal from the porous medium, and their impact on reservoir and caprock integrity are paramount. In this study, a dual-tubing string well completion technology was designed for cyclic injection and withdrawal of CO_2 (with or without another acid gas), and numerical simulations were performed using TOUGHREACT codes, to model the cyclic process and investigate the co-injection of SO_2 and H_2S (separately) with CO_2 in sandstone formations overlain by shale caprock. A novel technique of converting the volume fraction of minerals to their weight fraction was developed in this study, to evaluate the brittleness index of the sandstone reservoir and shale caprock during CO_2 geosequestration. The findings of the study indicate that the porosity and permeability increase for the CO_2 only and CO_2-H_2S injection cases, in the shale caprock; while for the CO_2-SO_2 injection case, porosity and permeability only decreased in the layers of the shale caprock contacted by SO_2 and due to anhydrite precipitation. In all the injection cases, the porosity and permeability of the sandstone reservoir decreased in a few layers directly below the perforation interval of the production zone. However, in other regions in the sandstone reservoir, the porosity and permeability increased for the CO_2 only and CO_2-H_2S injection cases. In contrast, for the CO_2-SO_2 co-injection case, porosity and permeability decreased in the layers of the sandstone rock contacted by SO_2. In all the CO_2 geosequestration cases, the brittleness of the shale and sandstone rocks investigated decreased slightly, except in the CO_2-SO_2 co-injection case where the brittleness of the sandstone rock decreased significantly. Based on the mineralogical composition of the formations in this study, co-injection of SO_2 gas with CO_2 gas, only decreased the brittleness index of the shale caprock slightly, but significantly decreased the brittleness of the sandstone reservoir.

Keywords: Cyclic, injection, withdrawal, geosequestration, brittleness index, dual-tubing string.

FORMATION INTEGRITY EVALUATION FOR GEOSEQUESTRATION OF CO_2 IN DEPLETED PETROLEUM RESERVOIRS UNDER CYCLIC STRESS CONDITIONS

By

Efenwengbe Nicholas Aminaho

Mamdud Hossain

Nadimul Haque Faisal

Reza Sanaee

October 2023

1. Introduction

Carbon dioxide (CO_2) geosequestration represents one of the most promising options for reducing atmospheric emissions of CO_2 (Bachu, 2002). It has been proposed as one solution to global climate change caused by the heat-trapping of anthropogenic gases in the atmosphere (Wei et al., 2015; Klokov et al., 2017; Liu et al., 2020). What is fascinating about geosequestration is that CO_2 can be stored underground in caverns (salt caverns or engineered caverns) or porous media (aquifer and depleted oil or gas reservoirs). For long-term storage of gases, underground storage in aquifers or depleted oil (or gas) reservoirs is preferable due to the large storage capacity of gases in aquifers and depleted oil or gas reservoirs (Panfilov, 2016). Nonetheless, caprock integrity ascertained based on its petrophysical, geochemical, and geomechanical properties is vital to ensuring safe and sustainable storage of CO_2 (Pearce et al., 2016; Liu et al., 2020).

Meanwhile, CO_2 geosequestration could involve a non-cyclic or cyclic process. On the one hand, the non-cyclic process entails the injection of CO_2 over a period, then stopping the injection and allowing the injected CO_2 to be trapped in the reservoir. On the other hand, the cyclic process of geosequestration involves the injection of CO_2 for some period (in some cases, withdrawing some of the injected CO_2 and leaving behind some amount of CO_2 in the reservoir), and repeating the process over the geosequestration period. Cyclic injection and withdrawal of CO_2 in reservoirs might be an effective technology to promote CO_2 utilization, as this technology would enable seasonal injection and withdrawal of CO_2. Following this approach, CO_2 can be produced from the reservoir when needed for electrochemical hydrogen production (Kim et al., 2018; Koomson et al., 2023), to produce renewable methanol (Sánchez-Díaz, 2017; Sollai et al., 2023; Wang et al., 2023), in CO_2 plume geothermal (CPG) systems for heat and power production (Schifflechner et al. 2022), or other forms of energy. Thus, the utilization of CO_2 for energy creation will reduce the world's reliance on fossil fuels (Wang et al., 2023). The cyclic injection and withdrawal of CO_2 will promote its storage and utilization.

CO_2 storage is possible by its different trapping mechanisms including solubility trapping, residual trapping, mineral trapping, and structural/stratigraphic trapping mechanisms (Sun et al., 2016). The purity of the injected fluid influences brine-rock interactions during CO_2 geosequestration. To save the cost of carbon capture and storage, small amounts of some other acid gases (such as SO_2 and H_2S) may be co-injected with CO_2. When the gas mixture comes into contact with water, each gas in the mixture exhibits a different level of solubility in water due to differences in their polarity and net dipole moment (López-Rendón and Alejandre, 2008; Miri et al., 2014; Wang et al., 2020). Theoretically, water (H_2O), SO_2, and H_2S are polar molecules (electrons are not shared equally between the atoms and there is an electronegativity difference between the bonded atoms), while CO_2 is a linear non-polar molecule and the electrons are shared equally between the atoms (López-Rendón and Alejandre, 2008; Wang et al., 2020). Thus, CO_2 has no net dipole moment (as the two C-O bond dipoles are equal in magnitude and cancel out each other); while the dipole moments of H_2S, SO_2, and H_2O are 0.97 Debye, 1.63 Debye, and 1.83 Debye, respectively (López-Rendón and Alejandre, 2008; Shen et al., 2015; Wang et al., 2020). Also, substances whose polarities (or net dipole moment) are similar tend to be more soluble in each other, and a polar substance is more soluble in a polar solvent than in a non-polar solvent (López-Rendón and Alejandre, 2008, Wang et al., 2020). Thus, for the same initial amount of CO_2 at the same temperature and pressure conditions, the solubility of H_2S or SO_2 in water is higher than that of CO_2 (López-Rendón and Alejandre, 2008; Miri et al., 2014; Wang et al., 2020). Moreover, it is expected that the solubility of SO_2 in water should be higher than that of H_2S at the same temperature and pressure conditions, as the dipole moment of SO_2 is closer to that of water. Also, the solubility of gases in water is dependent on temperature; as temperature increases, the solubility of CO_2, H_2S, or SO_2 in water increases (López-Rendón and Alejandre, 2008; Miri et al., 2014).

It is worth noting that a gas can separate from a mixture with non-polar gases, due to their difference in property. This concept drives the industrial separation of SO_2/CO_2 in ionic liquid or aqueous phase (Wang et al., 2020). However, the level of solubility of CO_2 or impurities in a brine-rock system or the separation of impurities from CO_2 might be different when gas mixtures are injected in a rock composed of different minerals, thereby resulting in the trapping of the dissolved gases in the aqueous phase for mineral precipitation. More or less fraction of each gas in the mixture might dissolve in the aqueous phase at different temperature and pressure conditions. So, the solubility trapping of CO_2 in a brine-rock system would depend on the initial mineralogical composition of the formation.

Residual trapping of CO_2 increases during cyclic CO_2 injection (Herring et al., 2016; Edlmann et al., 2019). During cyclic CO_2 injection, about 40-50% of CO_2 can be stored mainly through residual and solubility trappings in the porous medium (Abedini and Torabi, 2014). Water alternating gas (CO_2) and CO_2 cyclic injection strategies provide significantly higher effective CO_2 storage capacities compared to the continuous CO_2 injection strategy (Li et al., 2021). However, residually trapped CO_2 might reconnect with injected CO_2 mainly close to the large pore clusters in subsequent injection cycles, as observed during cyclic hydrogen (H_2) injections (Lysyy et al., 2023). Moreover, increased residual trapping of CO_2 during cyclic injection, could result in a reduction in effective permeability, thereby limiting flow and injectivity after several cycles of CO_2 injection (Edlmann et al., 2019).

The exposure of supercritical CO_2 in certain geologic materials may induce surface chemical reactions that are time-dependent (Herring et al., 2016). Thus, the surface chemical reactions can influence the pore structure of the rock, as dissolution-dominant reactions of rock minerals would result in increased porosity and permeability, while precipitation-dominant reactions would result in decreased porosity and permeability of the rock. Dissolution of primary minerals in carbonate rock increases the porosity and permeability of the rock (Wang et al., 2022, Fatima et al., 2021).

Bolourinejad and Herber (2014) conducted an experimental study on the storage of CO_2 and impurities in a depleted gas field in the northeast Netherlands. Experiments were conducted on Permian Rotliegend sandstone reservoir (no initial calcite content) and Zechstein caprock (anhydrite and carbonate component) core samples at 300 bar and 100 ^{0}C for 30 days. Anhydrite precipitation was observed in H_2S or SO_2 co-injection case with CO_2, as the geochemical reaction with the formation water provided additional sulphur; while anhydrite dissolved in the pure CO_2 injection case. Pyrite and halite precipitated for the CO_2-H_2S co-injection case. In the CO_2-SO_2 co-injection case, enhanced levels of dissolution of carbonate and feldspar minerals were observed due to the formation of sulphuric acid from the geochemical reaction. Furthermore, after CO_2 injection, the permeability of the reservoir samples increased by 10-30%; while the permeability of caprock samples increased by a factor of 3-10, which indicates a significantly higher increase in the permeability of the caprock samples compared to the sandstone reservoir rock samples. CO_2 co-injection with 5000 ppm H_2S (higher concentration of the gas impurity, different from the other cases with 100 ppm gas impurity) reduced the permeability of the reservoir and caprock samples significantly (due to significant halite precipitation and small amount of pyrite and anhydrite precipitation), while only minimal change in permeability (less than 3% increase in permeability of the sandstone reservoir sample, and an increase in permeability up to 30% in the caprock sample) was observed when the concentration of H_2S was reduced to 100 ppm as the dissolution of minerals resulted in corresponding precipitation of secondary minerals. It is worth noting that after 17 days of CO_2 co-injection with 100 ppm H_2S, the permeability of the reservoir and caprock samples decreased as the precipitation of halite dominated the dissolution of feldspar and carbonate minerals. However, over time, the mineral dissolution process dominated, resulting in an increase in permeability of the rock samples after 30 days. In the case of CO_2 co-injection with 100 ppm SO_2, the permeability of reservoir rock samples increased by a factor of 1.18 to 2.2, while the permeability of the caprock samples changed by a factor of 0.8 to 23 (permeability increased in caprock samples with a higher ratio of initial carbonate mineral concentration to

anhydrite content, due to the carbonate dissolution). The increase in the permeability of the sandstone reservoir could be attributed to the lack of calcite (mineral) in the initial composition of the rock. Thus, the release of Ca^{2+} from dolomite dissolution was not enough to precipitate a significant amount of anhydrite (which could have decreased the permeability of the reservoir rock in the CO_2-SO_2 case). So, the initial mineralogical composition of the rock, duration of the geochemical reactions, and concentration of impurities in a CO_2 gas stream in reservoir and caprock samples impact the amount of change in permeability of reservoir and caprock.

A similar experimental study was conducted by Aminu et al. (2018) to evaluate the effect of impurities on sandstone reservoir permeability. The impurities considered are NO_2, H_2S, and SO_2. The experiment was conducted at 70^0C and 140 bar for 9 months. They found that the effect of H_2S on the rock permeability is relatively small. CO_2 increased the reservoir rock permeability by 5.83%, while CO_2-H_2S increased it by 6.25%. CO_2 co-injection with SO_2 slightly decreased permeability by 6.25%; while CO_2 co-injection with NO_2 significantly decreased permeability by 41.67%. The changes in the rock permeability are significantly influenced by the dissolution and precipitation of existing rock minerals, as well as the precipitation of some secondary minerals. So, the CO_2-brine-rock interactions depend on the purity of the CO_2 gas as well as the initial mineralogical composition of the rocks. The changes in permeability and porosity result from the dissolution of these gases in water, thus reducing pH which enhances chemical reactions in the rock and results in the dissolution of minerals (such as ankerite, siderite, dolomite, etc.), and precipitation of minerals (such as pyrite, dawsonite, kaolinite, anhydrite, etc.) in the rock (Li et al., 2016; Pearce et al., 2016; Pearce et al., 2019).

Elwegaa et al. (2019) conducted a study on cyclic cold carbon dioxide injection for improved oil recovery from shale oil reservoirs. They found that injection of cold CO_2 increased both porosities and permeabilities of the core samples by up to 3.5% and 8.8%, respectively. The porosity and proportion of macropores of coal (carbonate-rich rock) increase after treatment on cyclical

injection of supercritical CO_2, as new pores were formed and some small pores possibly converted into macropores (Su et al., 2021). Moreover, the microporosity of sandstone increases during the cyclic wetting-drying process, similar to cyclic CO_2 injection, as the microstructure of the rock changes. The driving force of the changes in the microstructure of the sandstone is water-rock interaction including physical, mechanical, and chemical interactions (Ke et al., 2023). The chemical interaction that causes the dissolution and precipitation of some minerals in the rock can increase or decrease the porosity of the rock. For instance, in a study conducted by Badrouchi et al. (2022), after four CO_2 injection cycles, the effective porosity of the rock samples decreased, as the dissolved CO_2 could react with rock minerals and form precipitates that block some pores. These changes in the microstructure impact the petrophysical (porosity and permeability) and mechanical (elastic and strength parameters) properties of the rock. The strength and elastic (or deformation) parameters of the rock are dependent on its mineral compositions (Li et al., 2023). The change in the strength and elastic parameters (Young's modulus and Poisson's ratio) as the mineral compositions of the rock change during cyclic injection of CO_2 (Su et al., 2020; Xu et al., 2021) could impact the brittleness of the reservoir and cap rocks.

Elwegaa et al. (2019) conducted a study on cyclic cold carbon dioxide injection for improved oil recovery from shale oil reservoirs. They observed an increase in the brittleness indices of the core samples. However, in the study, cold CO_2 was injected into the shale rock (reservoir), and brittleness index was calculated mainly by the ratio of the sum of the volume fractions of quartz and dolomite (which are not the only major brittle minerals in the rock samples); and the brittleness ratio was evaluated based on dynamic elastic modulus and Poisson's ratio, which do not accurately reflect the brittleness of rocks (Meng et al., 2015; Zhang et al., 2016). Moreover, Lyu et al. (2018) developed a damage constitutive model for the effects of CO_2-brine-rock interactions on the brittleness of a low-clay shale (tested in a non-cyclic injection process). They found that the CO_2-brine-shale interactions in the soaked shale sample decreased the brittleness values.

Therefore, the development of a more robust mathematical model to evaluate the brittleness of reservoir and cap rocks during the non-cyclic and cyclic CO_2 injection process is paramount.

Previous studies have considered the impact of CO_2 and impurities (H_2S, SO_2, or NO_2) on porosity, permeability, and mineralogical changes in different rock lithologies, as well as the impact of pure CO_2-brine interaction on geomechanical properties and brittleness of rocks. Furthermore, several studies on the cyclic approach of CO_2 geosequestration have been based on CO_2 injection as a drainage-imbibition process in which case CO_2 is injected followed by water, from the same end of the rock sample and similar to water alternating gas approach of enhanced oil recovery; or periodic injection of CO_2 and producing from the other end of the reservoir (in a cartesian coordinate system) or observing the impact of the injected CO_2 in the reservoir. The cyclic injection-withdrawal of CO_2 during geosequestration is different in the present study.

In the present study, a novel approach of cyclic CO_2 geosequestration (with or without the addition of H_2S or SO_2 impurity) was developed to promote CO_2 utilization and storage by injecting CO_2 at the bottom of the well in a reservoir and producing CO_2 from the top part of the reservoir using the same well for both operations, to save cost and produce a purer form of CO_2. The proposed technology could be replicated on a laboratory scale by injecting CO_2 from one end of a water-saturated rock sample, followed by the injection of water from the other end of the rock sample [after the CO_2 injection period], making a cycle. This cycle can be repeated and therefore referred to as cyclic injection-withdrawal of CO_2 in the present study. This technology can be applied to several wells in the same reservoir, enabling the production of a purer form of CO_2 (with minimal chance of producing a large amount of brine together with the gas) as a larger amount of gas is few meters away (laterally) from the injection zone and at the top part of the reservoir; while multiphase mixture of CO_2-brine is found farther away from the injection well with a thin layer at the top of the reservoir having relatively low amount of CO_2 gas. Therefore, producing CO_2 gas from the same well used for injection, would save cost and enhance the production of a purer

form of CO_2 for the development of renewable resources or energy (CO_2 utilization for hydrogen and methanol production, as well as for heat and power generation).

Also, to the best knowledge of the authors, no study has been conducted to investigate the impact of CO_2 impurities (H_2S or SO_2) on the brittleness of reservoir or cap rocks during cyclic CO_2 injection and withdrawal from the same wells and enabling CO_2 storage at the same time. Therefore, it is against this background that the authors have conceived the idea to design a dual-tubing string well completion approach for cyclic injection and withdrawal of CO_2 and evaluate the impact of CO_2 impurities on the brittleness of reservoir and cap rocks under cyclic stress conditions, during CO_2 geosequestration. This study investigates the impact of CO_2 impurities on the porosity, permeability, geochemical composition, and brittleness index of a sandstone reservoir and shale caprock during underground injection, withdrawal, and storage of CO_2. This study adopted a novel technique for converting the volume fraction of minerals to weight fraction for the evaluation of the brittleness index of rocks.

2. Theoretical Framework

During CO_2 injection, stresses are induced in the rock as the cement that binds the rock grains are impacted. Thus, creating pathways for CO_2-brine-rock interaction in the [rock] cement and enhancing the dissolution of some of its minerals. Hence, resulting in deformation and a decrease in strength of the rock. The decrease in strength of the rock results in a change in the brittleness of the rock, as the rate of decrease in the tensile and compressive strengths of the rock, as well as changes in the rock minerals are different. Brittleness is the lack of ductility or plasticity of a material, while ductility is the property of a material that allows it to be drawn out by tension to a smaller section (Hucka and Das, 1974; Hou et al., 2018). In other words, brittle materials can hardly be drawn into shapes. Instead, they fracture or break when such an amount of stress is applied to them. Most rocks exhibit brittle behaviour. However, their degrees of brittleness vary by lithology and conditions subjected to during fluid-rock interactions.

Brittleness is a relative term as there are no accepted values of strength and elastic parameters ratios or brittle minerals ratio below which a material is considered ductile and above which it is considered as brittle (Hucka and Das, 1974). The brittleness of a material is compared by its brittleness index at one time or condition to another to ascertain whether the material has become more or less brittle. The factors that influence the brittleness of rocks include the type and composition of brittle minerals, the content and maturity of organic matter, and the formation temperature and confining pressure (Meng et al., 2015; Li, 2022). The brittleness index of rocks can be expressed based on rock strength parameters (Hucka and Das, 1974; Gong and Zhao, 2007; Meng et al., 2015; Li, 2022), elastic parameters (Rickman et al., 2008; Luan et al., 2014; Kang et al., 2020), and weight fraction of rock minerals (Jin et al., 2015; Guo et al., 2016; Kang et al., 2020; Li, 2022). Based on these parameters, the brittleness index of rocks is expressed as follows:

$$BI_1 = \frac{\sigma_c}{\sigma_t} \tag{1}$$

$$BI_2 = \frac{(\sigma_c - \sigma_t)}{(\sigma_c + \sigma_t)} \tag{2}$$

$$BI_3 = \frac{E}{v} \tag{3}$$

$$BI_4 = \frac{W_{quartz} + W_{feldspar} + W_{calcite} + W_{dolomite} + W_{pyrite} + W_{mica}}{W_T} \tag{4}$$

$$BI_5 = \frac{W_{quartz} + 0.49W_{feldspar} + 0.51W_{calcite} + 0.44W_{dolomite}}{W_T} \tag{5}$$

where σ_c represents uniaxial compressive strength and σ_t represents uniaxial tensile strength of the rock; E and v represent Young's modulus and Poisson's ratio of the rock, respectively; W and W_T represent weight (or mass) of individual mineral and total weight (or mass) of minerals in the solid part of the rock, respectively; and specifically, BI_5 is mineralogical brittleness index developed by Kang et al. (2020) based on the bulk modulus of brittle minerals. Generally, brittle

minerals include quartz, feldspar group of minerals, calcite, dolomite, pyrite, and mica. Fluid-rock interaction results in dissolution and precipitation of minerals, thereby altering the amount of brittle minerals in the rock. In the case of co-injection of CO_2 with SO_2, in the presence of water (H_2O) sulphates (or SO_4^{2-}) are formed, resulting in the precipitation of anhydrite ($CaSO_4$) and some amount of pyrite (FeS_2); while co-injection of CO_2 with H_2S in the presence of oxygen and increased iron (Fe) concentration (possibly due to the dissolution of siderite and/or ankerite) could result in the precipitation of pyrite (Hedayati et al., 2018) as follows:

$$Ca^{2+} + H_2SO_4 \rightarrow CaSO_4 + 2H^+ \quad (6)$$

$$2Fe^{2+} + 4H^+ + 4SO_4^{2-} \rightarrow 2FeS_2 + 7O_2 + 2H_2O \quad (7)$$

$$Fe^{+2} + 2H_2S + 0.5O_2 \rightarrow FeS_2 + H_2O + 2H^+ \quad (8)$$

Therefore, the co-injection of gases (H_2S, SO_2, etc.) during CO_2 geosequestration may impact the brittleness of porous rocks as brittle and non-brittle minerals are precipitated during the co-injection of CO_2 with different impurities. Hence, it is vital to evaluate the impact of CO_2 impurities on the brittleness of rocks during geosequestration.

3. Methodology

The research design involves numerical simulations. Numerical simulations were performed by modelling cyclic injection-withdrawal technology during CO_2 geosequestration. This strategy involves numerical simulations using sandstone formation as reservoir and shale formation as caprock, to model the process of cyclic injection-withdrawal of CO_2 in the reservoir. The results of the numerical simulations were analyzed for the brittleness index using the mathematical model developed by Aminaho and Hossain (2023). The mathematical model and the simulation approach are presented in this section.

3.1 Mathematical modelling

Change in the porosity of rocks is calculated based on mineral precipitation and dissolution, while the change in permeability is calculated from Carman-Kozeny relation, using the following equations (Xu et al., 2006; Xu et al., 2014):

$$\emptyset = 1 - \sum_{m=1}^{nm} fr_m - fr_u \quad (9)$$

$$k = k_0 \left(\frac{1-\emptyset_0}{1-\emptyset}\right)^2 \left(\frac{\emptyset}{\emptyset_0}\right)^3 \quad (10)$$

where, ϕ and k represent current porosity and permeability, ϕ_0 and k_0 represent initial porosity and permeability, parameters fr_m and fr_u represent volume fraction of mineral m in the rock (volume of mineral to volume of the medium including porosity) and volume fraction of non-reactive mineral, respectively. So, the output volume fraction of each mineral is the volume of the mineral divided by the volume of the medium including porosity (V_{frac}). Thus, the volume of each mineral divided by the total volume of the solid [part of the rock] is calculated as follows (Xu et al., 2014):

$$f_m = \frac{V_{frac}}{1-\emptyset_{med}} \quad (11)$$

where ϕ_{med} represents [current] porosity of the medium, and f_m represents the volume of mineral per volume of [the solid part of] the rock.

The mass fraction of composite materials has been calculated to determine their mechanical properties (Ezema et al., 2015) using their densities and volume fractions. Therefore, it is possible to determine the mass fraction of minerals in a rock using a similar approach. The mass fraction of each material that forms a composite structure is the mass of that material to the total mass of materials that form the structure. Similarly, the mass fraction of each mineral that forms a rock is the mass of each mineral to the total mass of minerals that form the rock and can be expressed as follows:

$$Mass\ fraction\ of\ a\ mineral, x_i = \frac{mass\ of\ the\ mineral,}{total\ mass\ of\ minerals\ in\ the\ rock,} = \frac{m_i}{\sum_{i=1}^{nm} m_i} \quad (12)$$

$$m = V\rho \quad (13)$$

$$x_i = \frac{v_i \rho_i}{\sum_{i=1}^{nm} v_i \rho_i} \quad (14)$$

where V and ρ represent the volume and density of the solid, respectively; v_i represents the volume fraction of each mineral in the solid part of the rock (same as f_m). Density can be expressed as molecular weight divided by molar volume.

$$\rho = \frac{\bar{M}}{\bar{V}} \quad (15)$$

Thus, the mass fraction becomes:

$$x_i = \frac{\frac{v_i \bar{M}_i}{\bar{V}_i}}{\sum_{i=1}^{nm} \frac{v_i \bar{M}_i}{\bar{V}_i}} \quad (16)$$

where $\bar{M}$ and $\bar{V}$ represent molecular weight (g/mol) and molar volume (m^3/mol) of mineral. Hence, the mineralogical brittleness index by a simple sum of brittle minerals becomes:

$$BI_{min} = \frac{\sum_{j=1}^{nB} \frac{v_j \bar{M}_j}{\bar{V}_j}}{\sum_{i=1}^{nm} \frac{v_i \bar{M}_i}{\bar{V}_i}} \quad (17)$$

where j represents each brittle mineral in the rock, i represents any mineral in the rock, and nB represents the number of brittle minerals in the rock.

To simplify the derived brittleness index equation, the same molar volume can be assumed for all minerals, depending on the mineralogical composition of the rock. However, some clay minerals such as smectite-Ca, smectite-Na, illite, and kaolinite may have larger mineral surface areas (Fatah et al., 2022) and significantly different molar volumes. Assuming equal molar volume of

minerals, the brittleness index in terms of the simple sum of brittle minerals in a rock can be expressed as:

$$BI_6 = \frac{\sum_{j=1}^{nB} v_j \bar{M}_j}{\sum_{i=1}^{nm} v_i \bar{M}_i} \quad (18)$$

Brittle minerals considered in this study are quartz, feldspar (as albite, k-feldspar, oligoclase, orthoclase, and anorthite), calcite, dolomite, pyrite, and mica (as muscovite). Their relative level of brittleness among themselves (brittle minerals) is not considered in the simple sum of brittle minerals approach given above. Thus, to consider their relative level of brittleness, the bulk modulus (Table 1) of the brittle minerals was incorporated into the equation using weighting coefficients (Table 2) following the mineralogical brittleness index developed by Kang et al. (2020).

Table 1: Bulk modulus of different brittle minerals (Fjaer et al., 2008).

Brittle mineral	Quartz	Feldspar	Calcite	Dolomite
Bulk modulus (GPa)	37.5	76	74	76-95

Table 2: Weighting coefficients of different brittle minerals (Kang et al., 2020).

Brittle mineral	Quartz	Feldspar	Calcite	Dolomite
Weighting coefficient	1	0.49	0.51	0.39-0.49/0.44

The mineralogical brittleness index, considering the bulk modulus of minerals, developed by Kang et al. (2020) is given as:

$$BI_{BMod} = \frac{W_Q + 0.49W_F + 0.51W_C + 0.44W_D}{W_T} \quad (19)$$

where W_Q, W_F, W_C, and W_D represent the weights of quartz, feldspar, calcite, and dolomite, respectively; W_T represents the total mineral weight. The brittleness index in this case considers only quartz (Q), feldspar (F), calcite (C), and dolomite (D) as brittle minerals, assuming the level of brittleness of pyrite and mica is negligible compared to other brittle minerals. Thus, in the present study, the brittleness index becomes:

$$BI_{bm} = \frac{\frac{v_Q\bar{M}_Q}{\bar{V}_Q}+\frac{0.49v_F\bar{M}_F}{\bar{V}_F}+\frac{0.51v_C\bar{M}_C}{\bar{V}_C}+\frac{0.44v_D\bar{M}_D}{\bar{V}_D}}{\sum_{i=1}^{nm}\frac{v_i\bar{M}_i}{\bar{V}_i}} \quad (20)$$

So, assuming the same molar volume of minerals in this present study, the brittleness index can be expressed as:

$$BI_7 = \frac{v_Q\bar{M}_Q+0.49v_F\bar{M}_F+0.51v_C\bar{M}_C+0.44v_D\bar{M}_D}{\sum_{i=1}^{nm}v_i\bar{M}_i} \quad (21)$$

The models developed in this study (accounting for the molar volume of each mineral and assuming the same molar volume for all minerals) are used to evaluate the mineralogical brittleness index of the sandstone reservoir and shale caprock before and after CO_2 geosequestration.

To test the statistical significance of differences in tests or observations at different stages or conditions, the concept of reliable change index (RCI) with 95% confidence (Blampied, 2016) can be adopted as follows:

$$RCI = 1.96(\sigma)\sqrt{2}\sqrt{(1-r)} \quad (22)$$

where, r and σ are Pearson correlation coefficient (or reliability index) and standard deviation of the variable dataset, respectively.

3.2 Numerical approach

This study employed the TOUGHREACT code for non-isothermal multiphase reactive geochemical transport (Xu et al., 2006), which was developed by incorporating reactive chemistry into TOUGH2 code for multiphase fluid and heat flow (Pruess, 2004). A detailed description of the TOUGHREACT code can be found in a study conducted by Zhang et al. (2010) and the program reference manual (Xu et al., 2014).

3.2.1 Model setup

A simple two-dimensional (2-D) radial well model was used in this study. The 2-D model is a vertically heterogeneous formation of 40 m thickness with a cylindrical geometrical configuration (Figure 1). In the vertical direction, the model domain is discretized into 20 regular increments with a 2 m constant spacing (Δz). The top and bottom model boundaries are close to flow. The top model layers represent a shale caprock, while the remaining model layers at the bottom represent reservoir rock(s). The model layers are shown in Table 3.

Table 3: Mesh generation of the model.

Rock formation	Vertical mesh number	Mesh thickness (m)
Shale caprock	6	2.0
Sandstone reservoir	14	2.0

In the horizontal direction, a 100 km radial distance was modelled with a radial grid spacing increasing logarithmically from the injection well. A total of 56 radial grid elements were generated. A large volume of 10^{30} m^3 is assigned to the outer grid element to represent an infinitive lateral boundary (a constant hydrostatic pressure boundary). The interface between the reservoir and caprock in this study is 12 m from the top of the caprock considered in this model The depleted petroleum reservoir considered in this study was assumed to be under a strong aquifer, such that a very large fraction of the hydrocarbon in the reservoir has been produced and the reservoir pore spaces were replaced by water. Therefore, the reservoir simulation is similar to CO_2 geosequestration in aquifers, which TOUGHREACT can handle effectively. Thus, the effect of hydrocarbon reactions with the injected gases and formation water were not considered in this study.

CO_2 only (also referred to as CO_2 alone, in this study) or impure CO_2 (containing H_2S or SO_2) injection was applied at the bottom of the well, and produced (or withdrawn) at the upper part of the well in the same reservoir (close to the caprock zone), to produce relatively pure CO_2 gas

(and limit the production of aqueous-phase fluid). The thickness of the injection portion is 8 m, while the thickness of the production portion is 6 m as shown in Figure 1.

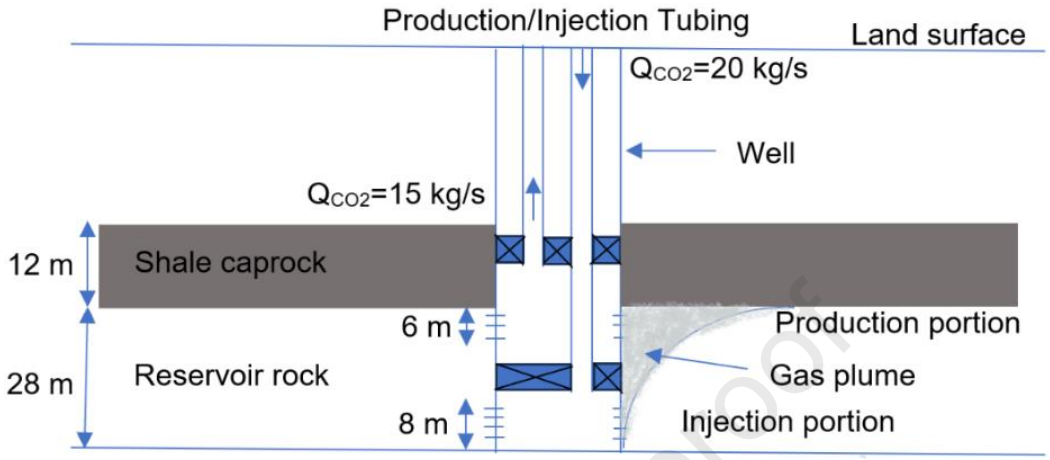

Figure 1: Cyclic injection-withdrawal of CO_2.

The initial reservoir and caprock temperature and pressure are 40^0C and 10 MPa (100 bar), respectively. The CO_2 injection-withdrawal profile is shown in Figure 2. The injection-withdrawal process was completed over seven (7) cycles. For each cycle, CO_2 gas (with or without H_2S/SO_2 gas) is injected (at the 8 m injection portion/zone) into the reservoir for a period of 10 years, using a CO_2 injection rate of 20 kg/s (with or without a gas impurity) and with a 0.025-mole fraction of H_2S or SO_2 (for the co-injection cases). The mole fraction of 0.025 for H_2S and SO_2 was selected as it is within the range of CO_2 co-capture from Pet Coke (SNC-Lavalin Inc., 2004). CO_2 injection is stopped for 3 months (0.25 year), then CO_2 is withdrawn from the reservoir at the rate of 15 kg/s (at the 6 m production portion/zone) over a period of 2 years and withdrawal is stopped for 3 months before the next cycle commences. So, each cycle lasted for 12.5 years. The longer period of production compared to the shut-in time is based on field applications of cyclic gas injection in reservoirs (Reeves, 2001). The hydrogeological parameters used in this study are shown in Table 4.

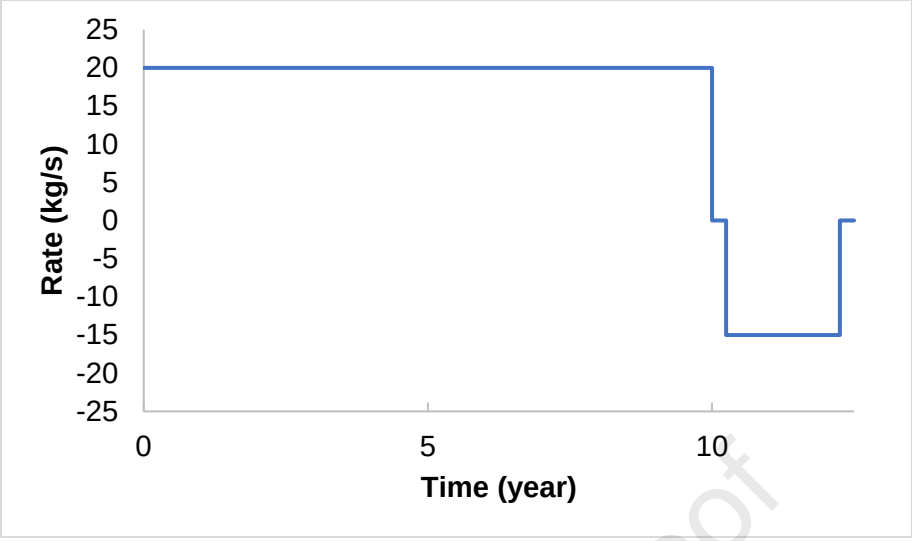

Figure 2: CO_2 injection-withdrawal profile.

Table 4: Hydrogeological parameters used in the simulation at formation temperature and pressure of 40^{0}C and 100 bar, respectively.

Parameters	Formation	
	Sandstone	Shale caprock
Porosity	0.34	0.07
Horizontal permeability (m^2)	$2.264x10^{-13}$	$2.264x10^{-16}$
Vertical permeability (m^2)	$2.264x10^{-14}$	$2.264x10^{-17}$
Pore compressibility (Pa^{-1})	$2.10x10^{-9}$	$2.10x10^{-9}$
Rock grain density (kg/m^3)	2600	2600
Formation heat conductivity (W/m ^{0}C)	2.51	2.51
Rock grain specific heat (J/kg ^{0}C)	920.0	920.0
Temperature (^{0}C)	40.0	40.0
Salinity (mass fraction)	0.06	0.06
Pressure (bar)	100	100
Initial gas saturation	0.00	0.00
CO_2 injection rate (kg/s)	20.0	-
CO_2 withdrawal rate (kg/s)	15.0	-
Relative permeability Liquid: Van Genuchten function $k_{rl} = \sqrt{S^*}\left\{1-\left(1-[S^*]^{1/m}\right)^m\right\}^2$ S_{lr}: residual water saturation m: exponent Gas: Corey $k_{rg} = (1-\hat{S})^2(1-\hat{S}^2)$ S_{gr}: residual gas saturation	$S^* = (S_l - S_{lr})/(1-S_{lr})$ $S_{lr} = 0.30$ $m = 0.457$ $\hat{S} = (S_l - S_{lr})/(1-S_{lr}-S_{gr})$ $S_{gr} = 0.05$	
Capillary pressure Van Genuchten function $P_{cap} = -P_0\left([S^*]^{-1/m}-1\right)^{1-m}$ S_{lr}: residual water saturation m: exponent	$S^* = (S_l - S_{lr})/(1-S_{lr})$ $S_{lr} = 0.03$ $m = 0.457$	
P_0: strength coefficient	19.61 kPa	19.61 kPa

The initial mineralogical composition of the sandstone reservoir was obtained and modified from Zhang et al. (2010), while the initial mineralogical composition of the shale caprock was obtained

and modified from Ma et al. (2019). The molar volumes of the minerals were obtained from Robie et al. (1967) and Wang et al. (2021), except the molar volumes of dawsonite, smectite-Ca and ankerite that were assumed. The molar volume of dawsonite was obtained from Marini (2007); the molar volume of smectite-Ca was estimated within the range of density of Smectites (2.6 g/cm^3) (Deer et al., 1966; Totten et al., 2002), while the molar volume of ankerite was estimated using a density of 2.97 g/cm^3 (Shafiq et al., 2022). The mineralogical compositions of the rocks are shown in Table 5.

Table 5: Initial volume fractions of the minerals and their molecular weight and molar volume.

Mineral name	Chemical formula	Molecular weight (g/mol)	Molar volume (cm^3/mol)	Sandstone formation (volume percent of solid)	Shale Caprock (volume percent of solid)
Illite	$K_{0.6}Mg_{0.25}Al_{1.8}(Al_{0.5}Si_{3.5}O_{10})(OH)_2$	383.899	138.900	2.80	65.30
Kaolinite	$Al_2Si_2O_5(OH)_4$	258.159	99.520	0.90	1.11
Smectite-Ca	$Ca_{0.145}Mg_{0.26}Al_{1.77}Si_{3.97}O_{10}(OH)_2$	365.394	140.536	0	6.96
Chlorite	$Mg_{2.5}Fe_{2.5}Al_2Si_3O_{10}(OH)_8$	634.648	210.260	2.70	6.40
Quartz	SiO_2	60.084	22.688	25.80	8.00
K-feldspar	$KAlSi_3O_8$	278.33	108.900	23.30	2.80
Albite	$NaAlSi_3O_8$	262.222	100.070	41.50	3.20
Calcite	$CaCO_3$	100.087	36.934	3.00	0.80
Pyrite	FeS_2	119.98	23.940	0	1.43
Dolomite	$CaMg(CO_3)_2$	184.401	64.341	0	0
Anhydrite	$CaSO_4$	136.142	45.940	0	4.00
Siderite	$FeCO_3$	115.856	146.800	0	0
Alunite	$KAl_3(OH)_6(SO_4)_2$	414.214	69.522	0	0
Ankerite	$CaMg_{0.3}Fe_{0.7}(CO_3)_2$	206.48	58.520	0	0
Dawsonite	$NaAlCO_3(OH)_2$	143.995	28.018	0	0
Magnesite	$MgCO_3$	84.314	29.378	0	0
Smectite-Na	$Na_{0.290}Mg_{0.26}Al_{1.77}Si_{3.97}O_{10}(OH)_2$	366.25	132.510	0	0
Hematite	Fe_2O_3	159.692	30.274	0	0
Anorthite	$CaAl_2Si_2O_8$	278.206	100.790	0	0
Muscovite	$KAl_2(AlSi_3O_{10})(F,OH)_2$	398.306	140.710	0	0
Oligoclase	$CaNa_4Al_6Si_{14}O_{40}$	1327.094	502.480	0	0

Before the simulation of reactive transport, a batch geochemical modelling of water-rock interaction was performed to obtain an aqueous-phase chemical composition similar to the composition of a typical formation brine. So, synthetic brine formulated by AL-Ameri et al. (2016) with very little amount of other necessary ions based on the mineral compositions considered in the simulations was used. The synthetic brine was equilibrated separately for the different formations and injection conditions considered, in the presence of the primary minerals listed in

Table 5. The batch geochemical modelling was conducted for 100 years to obtain a quasi-stable (or nearly steady-state) aqueous solution composition as shown in Table 6.

Table 6: Initial chemical composition of the formation water at formation conditions of 40^{0}C and 100 bar.

Component	Concentration (mol/kg H_2O)	
	Sandstone formation	**Shale caprock**
Ca^{2+}	4.7137E-01	4.8163E-01
Mg^{2+}	1.0038E-01	9.7547E-02
Na^{+}	2.5868E+00	2.6006E+00
K^{+}	2.8166E-03	3.3113E-03
Fe^{2+}	4.9784E-04	2.7904E-08
SiO_2 (aq)	2.9555E-03	1.3991E-03
HCO_3^-	2.1733E-03	1.2688E-04
SO_4^{2-}	3.6425E-03	1.7486E-02
AlO_2^-	1.3611E-11	6.1835E-11
Cl^-	3.7245E+00	3.7264E+00
pH	6.1989	7.3919

Dissolution and precipitation of minerals are considered under kinetic conditions based on the rate law (Lasaga et al., 1994) expressed as:

$$r_n = \pm k_n A_n \left[1 - \left(\frac{Q_n}{K_n}\right)^{\theta}\right]^{\eta} \quad (23)$$

where k_n is the rate constant (in moles per unit mineral surface area and unit time) which is temperature-dependent, A_n denotes the specific reactive surface area per kilogram H_2O, Q_n is the reaction quotient, K_n is the equilibrium constant for the mineral-water written for the destruction of one mole of mineral n, and η represents kinetic mineral index. The parameters θ and η which are determined by experiments, are more often assumed to equal to one. Positive values of r_n indicate dissolution, while negative values indicate precipitation.

A general form of species-dependent rate constants implemented in TOUGHREACT is expressed as:

$$k = k_{25}^{nu} exp\left[\frac{-E_a^{nu}}{R}\left(\frac{1}{T} - \frac{1}{298.15}\right)\right] + \sum_i k_{25}^{i} exp\left[\frac{-E_a^{i}}{R}\left(\frac{1}{T} - \frac{1}{298.15}\right)\right] \prod_j a_{ij}^{n_{ij}} \quad (24)$$

where superscripts or subscripts i represents the additional mechanism index, and j represents the species index involved in one mechanism that could be primary or secondary species.

In this study, calcite and anhydrite are assumed to react with aqueous species at local equilibrium. This is because the reaction rates of calcite and anhydrite are typically quite rapid (Zheng et al., 2009). The kinetic parameters were taken from Xu et al. (2006) and Zhang et al. (2010) and are shown in Table 7.

Table 7: List of parameters for calculating the kinetic rate of minerals.

Mineral name	Initial reactive surface area (cm^2/g)	Neutral mechanism		Acid mechanism			Base mechanism		
		K_{25} (mol/m^2s)	E_a (kJ/mol)	K_{25} (mol/m^2s)	E_a (kJ/mol)	n(H^+)	K_{25} (mol/m^2s)	E_a (kJ/mol)	n(H^+)
Calcite	Assumed in equilibrium								
Anhydrite	Assumed in equilibrium								
Quartz	9.8	1.0233E-14	87.7						
Kaolinite	151.63	6.9183E-14	22.2	4.8978E-12	65.90	0.777	8.9125E-18	17.90	-0.472
Illite	151.63	1.6596E-13	35.00	1.0471E-11	23.6	0.34	3.02E-17	58.9	-0.40
Pyrite	12.87	2.8184E-05	56.90 $n_{O2(aq)}$=0.5	3.02E-08	56.9	n_{H+}=-0.5 n_{Fe3+}=0.5			
K-feldspar	9.8	3.8905E-13	38.0	8.7096E-11	51.7	0.5	6.3096E-22	94.1	-0.823
Dolomite	9.8	2.9512E-08	52.20	6.4565E-04	36.1	0.5			
Siderite	9.8	1.2598E-09	62.76	6.4565E-04	36.1	0.5			
Ankerite	9.8	1.2598E-09	62.76	6.4565E-04	36.1	0.5			
Albite	9.8	2.7542E-13	69.80	6.9183E-11	65.0	0.457	2.5119E-16	71.0	-0.572
Muscovite	9.8	3.160E-13	58.6						
Hematite	12.87	2.5119E-15	66.2	4.0738E-10	66.2	1.0			
Chlorite	9.8	3.020E-13	88.0	7.7624E-12	88.0	0.5			
Oligoclase	9.8	1.4454E-13	69.8	2.1380E-11	65.0	0.457			
Magnesite	9.8	4.5709E-10	23.5	4.1687E-07	14.4	1.0			
Dawsonite	9.8	1.2598E-09	62.76	6.4565E-04	36.1	0.5			
Smectite-Na	151.63	1.6596E-13	35.0	1.0471E-11	23.6	0.34	3.0200E-17	58.9	-0.40
Smectite-Ca	151.63	1.6596E-13	35.0	1.0471E-11	23.6	0.34	3.0200E-17	58.9	-0.40
Alunite	9.8	1.0000E-12	57.78				1.0000E-12	7.5	-1.00
Anorthite	9.8	1.5000E-14	18.4						

A temperature of 40^0C was used in the reservoir which may represent shallow formation temperature at a depth of about 800 m, given a land surface temperature of 16^0C and a geothermal gradient of 30^0C/km. The temperature in the reservoir and cap rocks are assumed to be initially the same as the rock thickness considered in the simulation is only 40 m. Also, the numerical simulations were conducted under isothermal condition.

3.2.2 Simulations

Three groups of numerical simulations were performed (as shown in Table 8) to investigate the effect of CO_2 injection or CO_2 co-injection with other gases (H_2S or SO_2) on the petrophysical

(porosity and permeability) and geochemical (aqueous composition and mineral dissolution/precipitation) changes of the rocks, and evaluate the brittleness of the rocks during the cyclic technique of CO_2 geosequestration.

Table 8: Three groups of simulations in this study.

Simulation groups	Injection scenarios	Formation	Formation salinity
1	CO_2 only	Sandstone and shale	0.06
2	CO_2 and H_2S	Sandstone and shale	0.06
3	CO_2 and SO_2	Sandstone and shale	0.06

3.3 Model Validation

The numerical simulations performed and the mathematical model adopted for the evaluation of brittleness index of rocks in this study were validated using experimental data published by Mavhengere et al. (2022) on the influences of SO_2 contamination in long-term supercritical CO_2 treatment on the physical and structural characteristics of sandstone rock. Mavhengere et al. (2022) conducted two types of storage experiments on sandstone core samples (Cenomanian Sandstone, ZG and Siltstone lateral seal Aptian Sandstone, ZC) from Zululand Basin in South Africa, using pure CO_2 gas (purity of 99.9% by weight); and another case using a mixture of 99% (weight) CO_2 and 1% (weight) SO_2 gas. Non-stirred Teflon lined N4766 Parr reactors were used to simulate geosequestration conditions of 17.5 MPa and 346 K for the ZC core samples, and 10 MPa and 316K for the ZG core samples for 2 months. X-ray diffraction (XRD) analyses were conducted on the samples before and after treatment with CO_2 or CO_2-SO_2 mixture to investigate any mineral phase alterations. The ZC core sample exhibited mineral phase alteration after treatment (fluid-rock interaction) similar to the sandstone rock in the present study. Therefore, to validate the mathematical models adopted in the present study, to evaluate the impact of contaminant (SO_2) in CO_2 on the brittleness index of sandstone, the mineral phases (weight fraction) of the ZC core samples (shown in Table 9) were incorporated into existing models that are based on simple weight fraction of brittle minerals (Jin et al., 2015; Guo et al., 2016; Li, 2022) and weight fraction considering the relative brittleness of brittle minerals (Kang et al., 2020). In

this case, the brittle minerals are quartz, plagioclase (feldspar), calcite, pyrite, and orthoclase (feldspar).

Table 9: ZC and ZG core samples XRD results before and after $ScCO_2$-water and $ScCO_2$-SO_2-water treatment (Mavhengere et al., 2022).

Sample	Quartz (wt. %)	Plagioclase (wt. %)	Smectite (wt. %)	Calcite (wt. %)	Pyrite (wt. %)	Stilbite (wt. %)	Diopside (wt. %)	Gypsum (wt. %)	Orthoclase (wt. %)
ZC untreated	44.1	44.7	1.0	3.5	0.4	3.6	2.7	0.0	0.0
ZC CO_2 treated	47.5	42.5	2.5	1.7	0.4	2.7	2.8	0.0	0.0
ZC CO_2-SO_2 treated	49.1	28.6	11.8	0.0	0.8	4.9	2.3	2.5	0.0
ZG untreated	21.5	46.0	22.2	0.0	0.0	2.0	0.0	0.0	8.3
ZG CO_2 treated	22.3	50.5	16.3	2.9	0.0	4.8	0.0	0.0	3.2
ZG CO_2-SO_2 treated	26.1	53.4	12.1	2.3	0.0	0.0	0.0	0.0	6.2

4. Results and Discussion

4.1 Impact of impurities on porosity, permeability, and geochemical composition of reservoir and cap rocks during CO_2 injection, withdrawal, and storage

The supercritical CO_2 fluid (referred to as 'gas' in this study for simplicity) is injected or co-injected with H_2S (or SO_2) near the bottom of the sandstone reservoir and withdrawn near the top of the reservoir, in a cyclic process (in a total of seven cycles). The injected fluid migrates rapidly upward by buoyant forces. After every cycle of injection, a small fraction of CO_2 gas is trapped in the reservoir as residual gas; while the mobile gas continues to migrate into the shale caprock by the action of buoyant forces. At the same time, some amount of the gas continues to dissolve into brine (formation water). Hence, the residual gas slowly disappears at the bottom of the reservoir. After some time, most of the free CO_2 gas accumulates in the shale caprock layers, a few metres from the reservoir-caprock interface, and spreads laterally. The SO_2 gas front is far behind that of CO_2 gas compared to the front of H_2S gas with respect to CO_2 gas as shown in Figure 3. This is because the solubility of SO_2 gas in formation water is higher than that of H_2S and CO_2. This difference in their solubility level can be attributed to their difference in polarity and net dipole moment, as the net dipole moment of SO_2 is closer to that of water molecule, compared to the closeness of the net dipole moment of H_2S to water molecule (López-Rendón and Alejandre, 2008; Miri et al., 2014; Wang et al., 2020). However, some amount of H_2S gas and SO_2 gas

remain in the reservoir even after the seventh cycle, as they continue to be replenished due to the cyclic injection process (Figure 4).

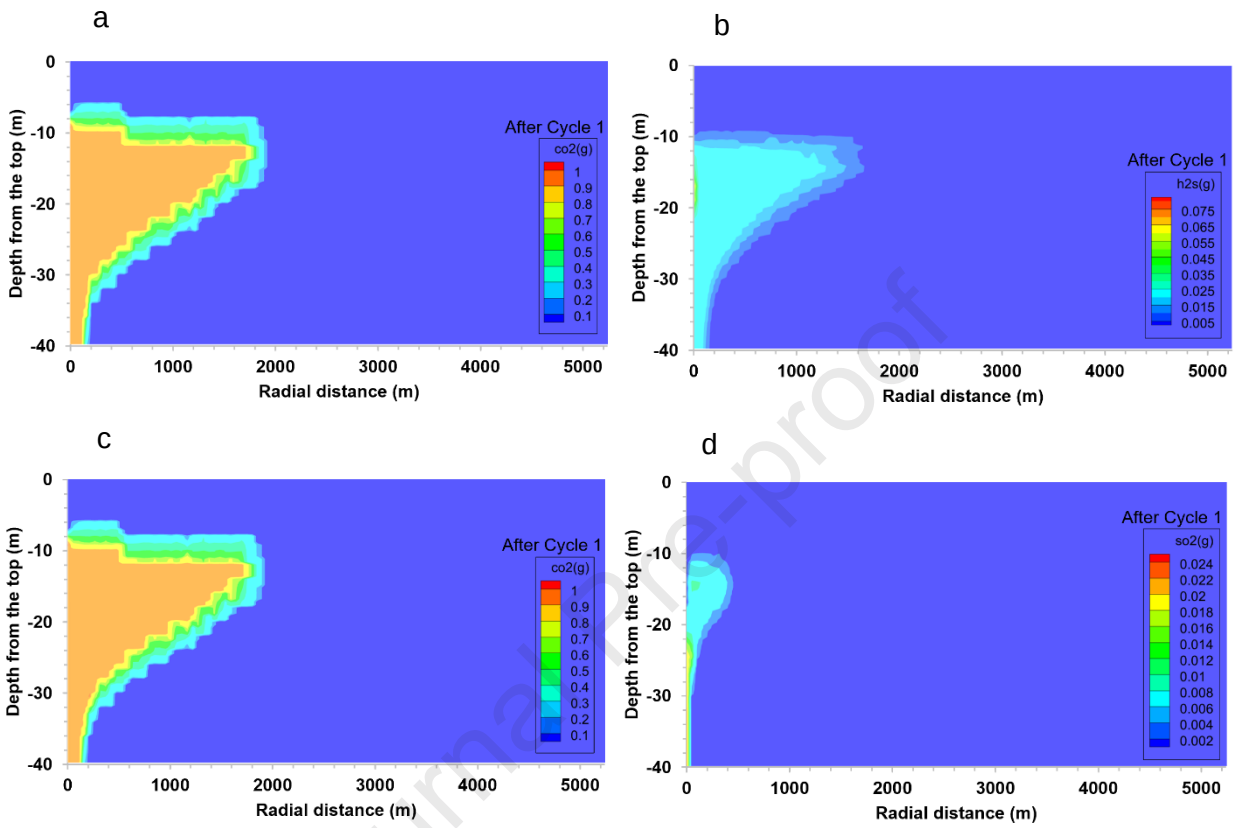

Figure 3: Gas front of (a) CO_2 in CO_2-H_2S (b) H_2S (c) CO_2 in CO_2-SO_2 (d) SO_2 in cyclic process

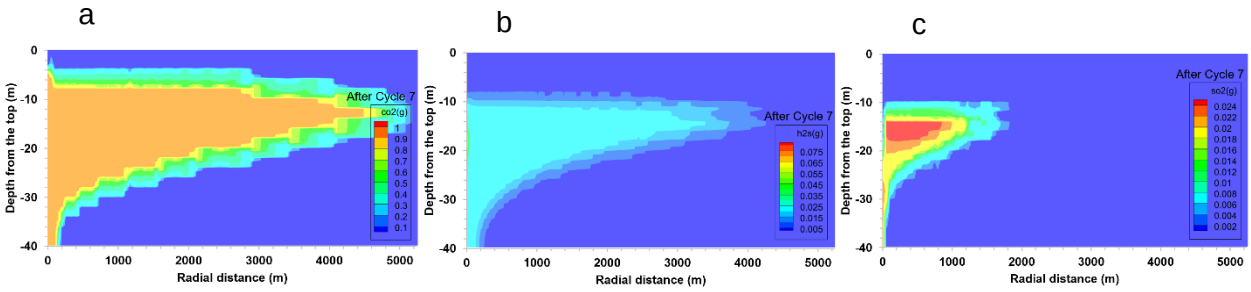

Figure 4: (a) CO_2 gas (b) H_2S gas (c) SO_2 gas in the formation after seven cyclic injection-withdrawal process.

Figure 4 shows that H_2S gas hardly penetrated up to 4 m vertical thickness of the shale caprock, while SO_2 gas only penetrated up to 2 m vertical thickness of the caprock after seven (7) cyclic

injection-withdrawal of CO_2 stream. Only CO_2 gas penetrated over 8 m vertical thickness of the shale caprock during the period of geosequestration.

There is no notable difference in the distribution of total dissolved carbon (TDC) for the geosequestration cases (after seven cyclic injection-withdrawal process of fluid), as the initially displaced formation water during supercritical fluid injection flows towards the injection-production well and provides sufficient pressure needed for the gas production. Thus, convective mixing of the CO_2 with formation water during the withdrawal process might have made the TDC for all the injection cases similar. It is also possible that some residually trapped CO_2 might have reconnected with the injected CO_2 in subsequent injection cycles mainly close to the large pore clusters, as Lysyy et al. (2023) observed for hydrogen during cyclic hydrogen (H_2) injections. The concentration of dissolved CO_2 increased up to 0.9 mol/kg H_2O in the two-phase region due to the CO_2 gas migration (Figure 5). The dissolution of the injected CO_2 (with or without cases of H_2S or SO_2 gas co-injection) in the surrounding formation water yields H_2CO_3, HCO_3^-, and CO_3^{2-}, and decreases pH (increases acidity). The pH profiles of all the injection cases are similar, as shown in Figure 6. However, for the CO_2-SO_2 co-injection case, the pH of the reservoir at and near the perforations in the production zone is relatively very low compared to the other injection cases. This could be attributed to severe calcite dissolution in those regions resulting in very low pH. In other regions of the formations, the pH values are similar for all the injection cases.

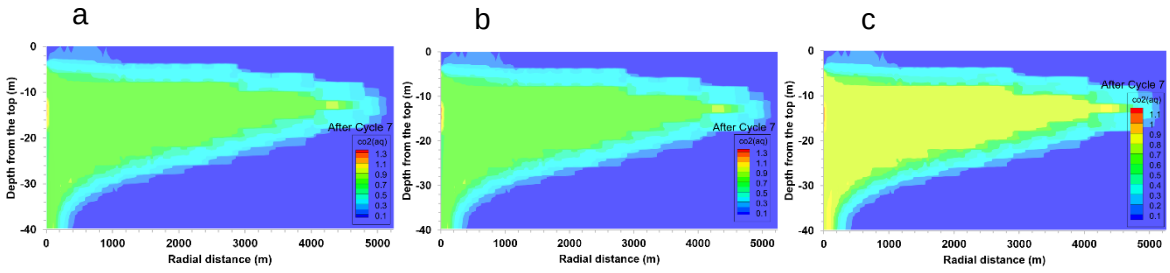

Figure 5: TDC for (a) CO_2 alone (b) CO_2-H_2S (c) CO_2-SO_2 cases in the formation after seven (7) cyclic injection-withdrawal process.

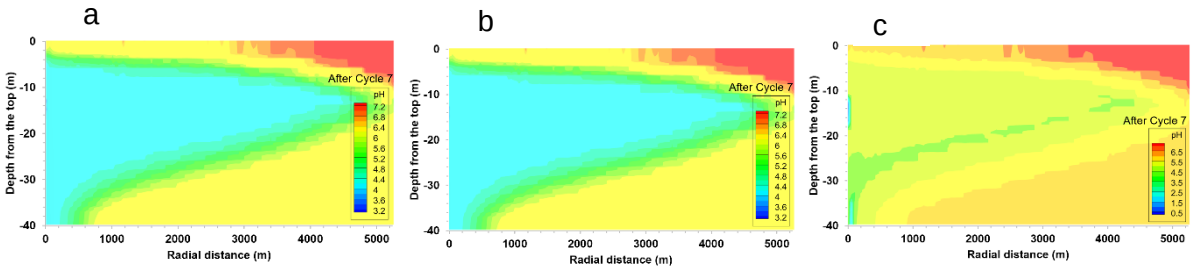

Figure 6: pH for (a) CO_2 alone (b) CO_2-H_2S (c) CO_2-SO_2 cases in the formation after seven (7) cyclic injection-withdrawal process.

The low pH induces the dissolution and precipitation of minerals. Dissolution of the minerals increases concentrations of cations including Na^+, Ca^{2+}, Mg^{2+}, and Fe^{2+}, which then form aqueous complexes with the carbonate ions and further precipitation of minerals (including secondary minerals). Examples of such aqueous complexes are $NaHCO_3$, $CaHCO_3^+$, $MgHCO_3^+$, and $FeHCO_3^+$; and examples of precipitated secondary minerals are ankerite, dawsonite, siderite, smectite-Na, pyrite, and anhydrite (CO_2-SO_2 co-injection case). As the aqueous complexes are formed, more CO_2 goes into the solution and enhances solubility trapping. However, mineral trapping of CO_2 was not considered in this study as it is a slow process that occurs over hundreds to thousands of years, while the numerical simulations in this study were performed up to a maximum of 87.5 years. So, the CO_2 trapping mechanisms in the present study are structural/stratigraphic trapping (caprock), residual trapping, and solubility trapping.

Minerals such as anhydrite, albite, chlorite, illite, k-feldspar, and kaolinite in the shale formation dissolve in the two-phase region and near the front of the single aqueous-phase zone. The mineral reactions are consistent with the findings in the study conducted (up to 5000 years of sequestration) by Ma et al. (2019). Calcite, albite, chlorite, and k-feldspar in sandstone reservoir dissolve in the two-phase region and near the front of the single aqueous-phase zone. On the other hand, calcite, ankerite, quartz, siderite, smectite-Ca, smectite-Na, and small amounts of hematite and pyrite precipitated in the shale caprock; while illite, kaolinite, quartz, and smectite-Na precipitated in the sandstone reservoir during the cyclic injection and withdrawal of CO_2 (Figures 7 to 10). For the CO_2-H_2S co-injection case, pyrite precipitated in the sandstone reservoir and shale caprock; while for the CO_2-SO_2 co-injection case, anhydrite, pyrite, and a small amount

of dawsonite precipitated in the shale and sandstone formations. This result is in line with the findings of Zhang et al. (2010), and the precipitation of ankerite and siderite can be attributed to the fact that Fe^{2+} is required and supplied by the dissolution of iron-bearing minerals such as chlorite. Very large amount of calcite dissolved in the CO_2-SO_2 case compared to the other injection cases. In fact, complete to significant dissolution of calcite mineral was observed at and near the perforations in the production zone for all the injection cases. Thus, erosion of the calcite mineral during CO_2 withdrawal resulted in the deposition of some of the calcite mineral in reservoir layers directly below the perforation interval in the production zone. Consequently, the porosity of those few reservoir layers directly below the perforation interval in the production zone decreased during the CO_2 geosequestration. Moreover, the large amount of calcite dissolution at and near the perforation interval of the production zone resulted in significant precipitation of anhydrite in that region for the CO_2-SO_2 co-injection case. Changes in the composition (volume fraction of the solid rock) of calcite, anhydrite, and pyrite during the cyclic process of the CO_2 geosequestration are shown in Figure 7.

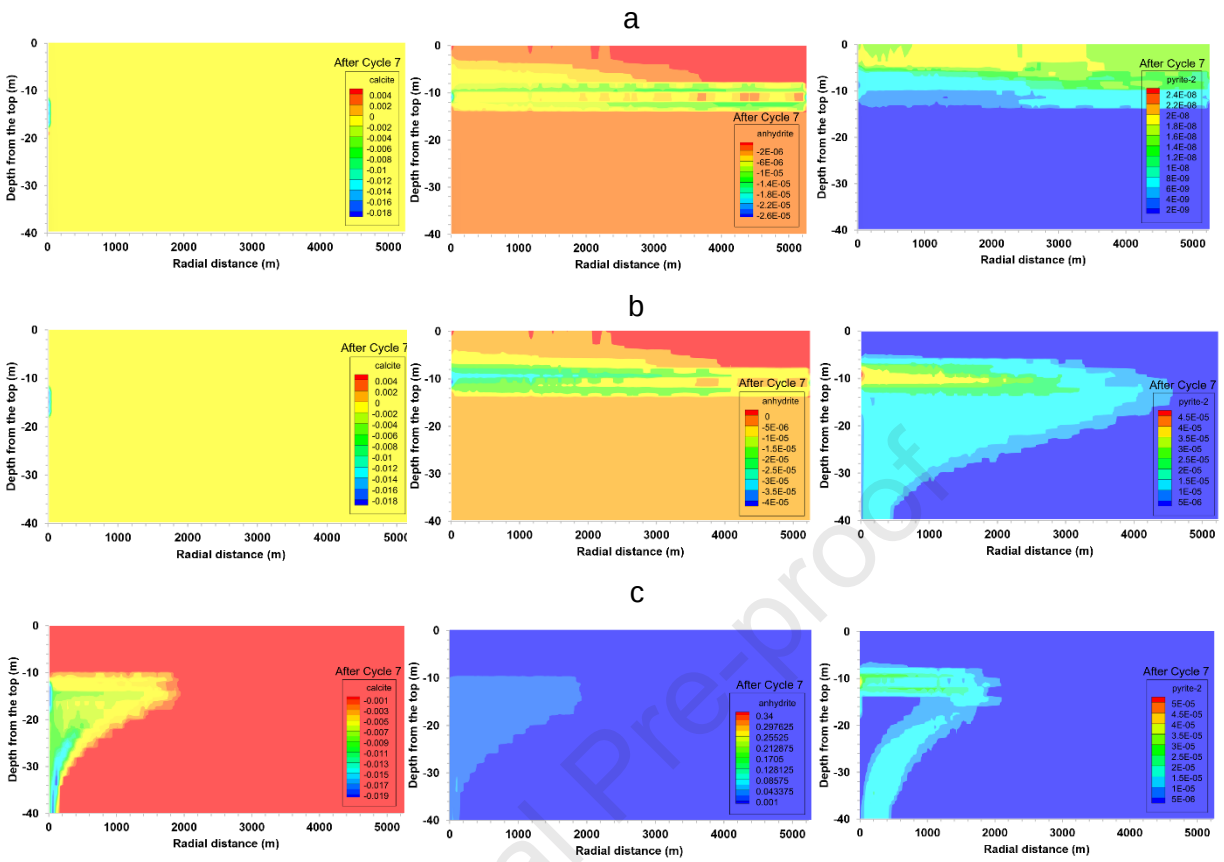

Figure 7: Changes in calcite, anhydrite, and pyrite composition for (a) CO_2 alone (b) CO_2-H_2S (c) CO_2-SO_2 injection cases in the formations after seven (7) cyclic injection-withdrawal process.

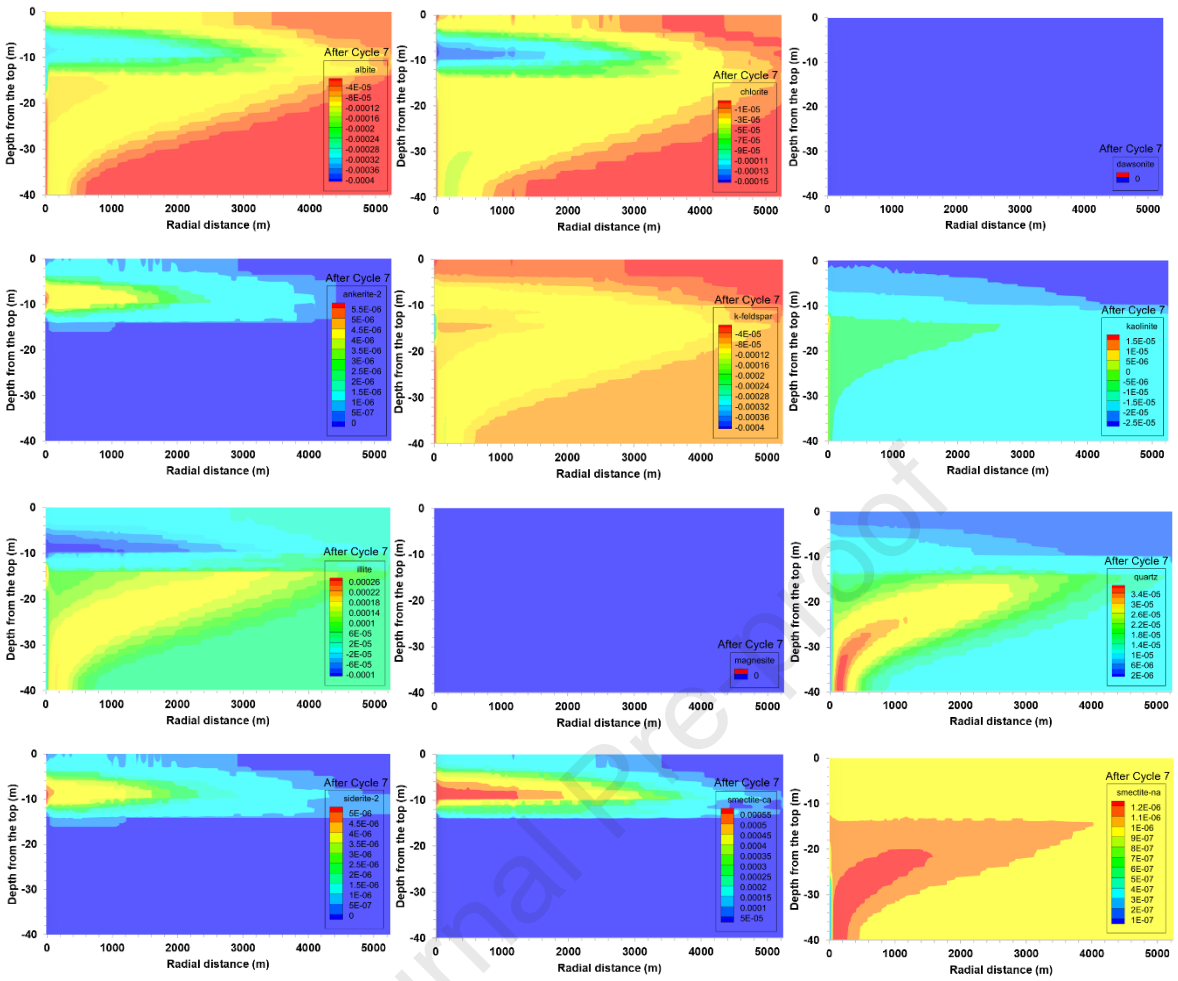

Figure 8: Mineral dissolution and precipitation in the sandstone reservoir and shale caprock for the CO_2 alone case after seven (7) cycles of injection and withdrawal.

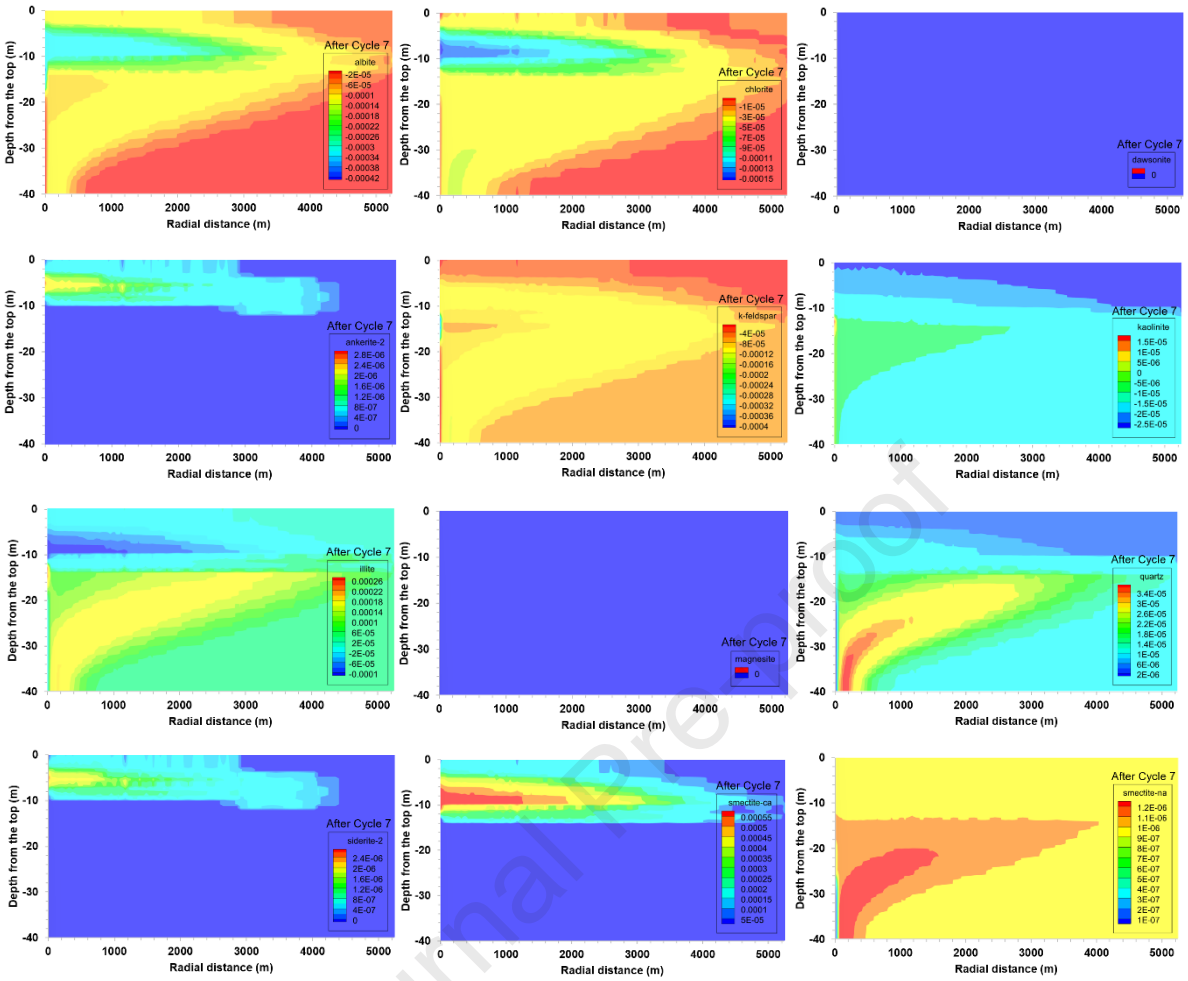

Figure 9: Mineral dissolution and precipitation in the sandstone reservoir and shale caprock for the CO_2-H_2S case after seven (7) cycles of injection and withdrawal.

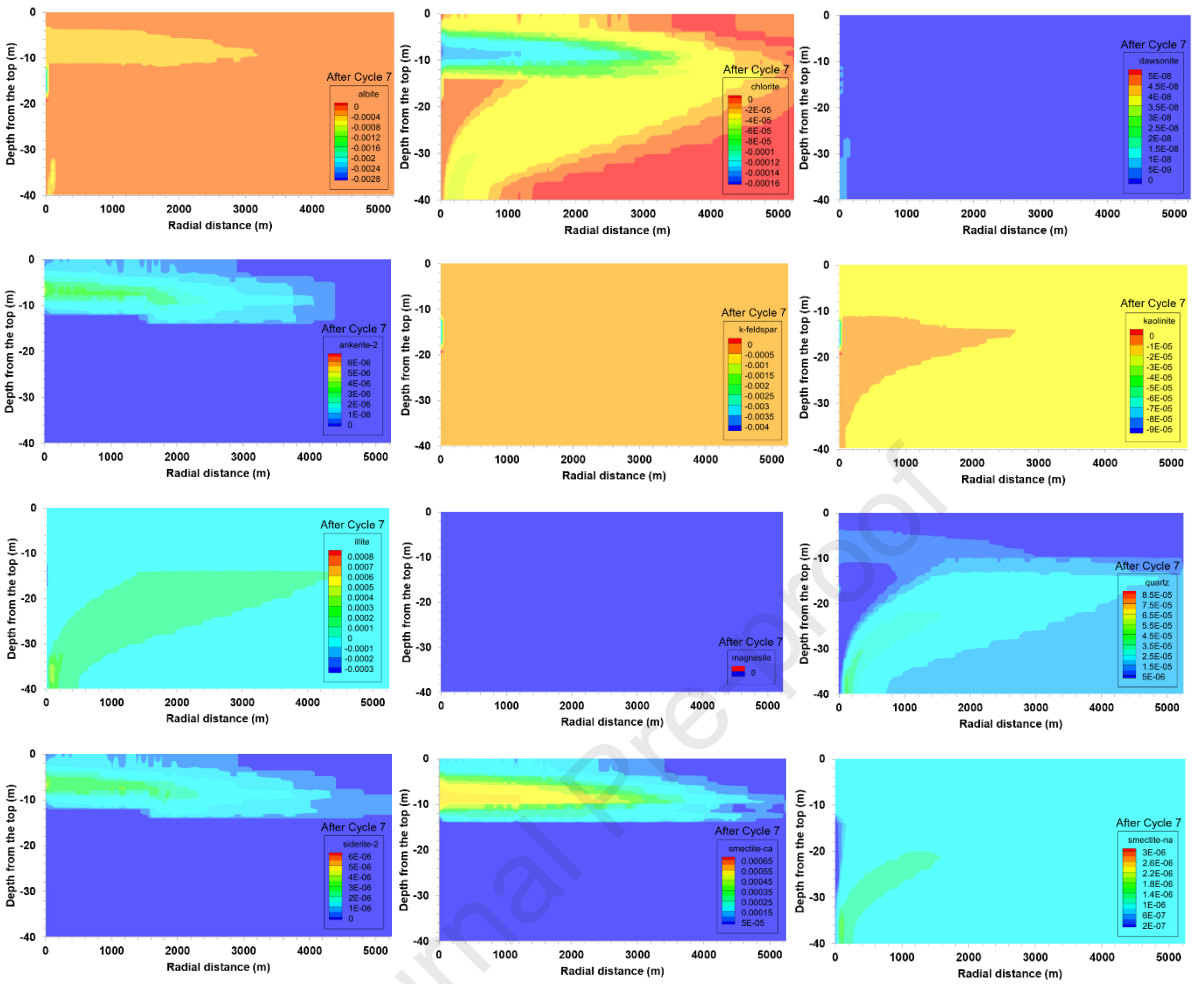

Figure 10: Mineral dissolution and precipitation in the sandstone reservoir and shale caprock for the CO_2-SO_2 case after seven (7) cycles of injection and withdrawal.

Changes in porosity are calculated from variations in the volume fraction of the minerals, while the permeability ratios are calculated by the changes in the porosity using the Kozeny-Carman relation. In the two-phase region, due to dominant mineral dissolution caused by low pH, porosity increases slightly in the shale and sandstone rocks, in the cases of CO_2 alone and CO_2-H_2S co-injection, while in the case of CO_2-SO_2 co-injection, porosity increases in most part of the shale rock (except in the layer contacted by SO_2 and where anhydrite precipitated) and decreases in the sandstone reservoir due to anhydrite precipitation.

For the CO_2-SO_2 co-injection case, at the perforations in the production zone, the reservoir porosity increased and it is between 0.36120 and 0.36672, while in every other region where SO_2

dissolved in water, porosity decreased (the lowest porosity observed is 0.32496). Beyond the regions contacted by SO_2 (mainly dissolved CO_2), porosity increased up to 0.34891 (the corresponding permeability increase is 11.05%). In the shale caprock, porosity decreased in the layer contacted by SO_2 (about 2 m vertical thickness); in other areas of the caprock contacted mainly by CO_2, porosity increased slightly. For the CO_2-H_2S co-injection case, at the perforations in the production zone, porosity increased and it is between 0.36018 and 0.36031. From the lower perforation layer at the perforation zone down to 2-6 m vertical thickness and up to about 7 m lateral distance in the reservoir, porosity decreased. This decrease in porosity can be attributed to the deposition of fines or minerals due to the erosion of some minerals or rock materials in the production zone during CO_2 gas withdrawal from the perforation interval. This result is in line with the submission of Saeedi et al. (2011) that rocks susceptible to formation damage (including fines migration) may experience reduced injectivity during cyclic CO_2-brine injection, even though the level of damage would stabilize after several cycles of injection. However, porosity increased in other areas contacted by CO_2. For the CO_2 alone case, at the perforations in the production zone, porosity increased and it is between 0.36019 and 0.36032. From the lower perforation layer at the perforation zone down to 2-6 m vertical thickness and up to about 9m lateral distance in the reservoir, porosity decreased, while porosity increased in other areas contacted by CO_2. In all the injection cases, the porosity and permeability of the shale caprock decreased slightly in the regions that were not contacted by any of the gases. The porosity and corresponding changes in the permeability of the formations are shown in Table 10 and Figure 11.

Table 10: Porosity and permeability ratio of the formations after seven (7) cycles of CO_2 injection and withdrawal.

Formation type	Petrophysics	After Cycle 7		
		CO_2	CO_2-H_2S	CO_2-SO_2
Shale caprock	Porosity	0.06998-0.07013	0.06998-0.07015	0.06979-0.07009
	Permeability ratio	0.99904-1.00590	0.99903-1.00660	0.99078-1.00400
Sandstone reservoir	Porosity	0.33470-0.36032	0.33475-0.36031	0.32496-0.36672
	Permeability ratio	0.93881-1.26700	0.93943-1.26680	0.83462-1.36290

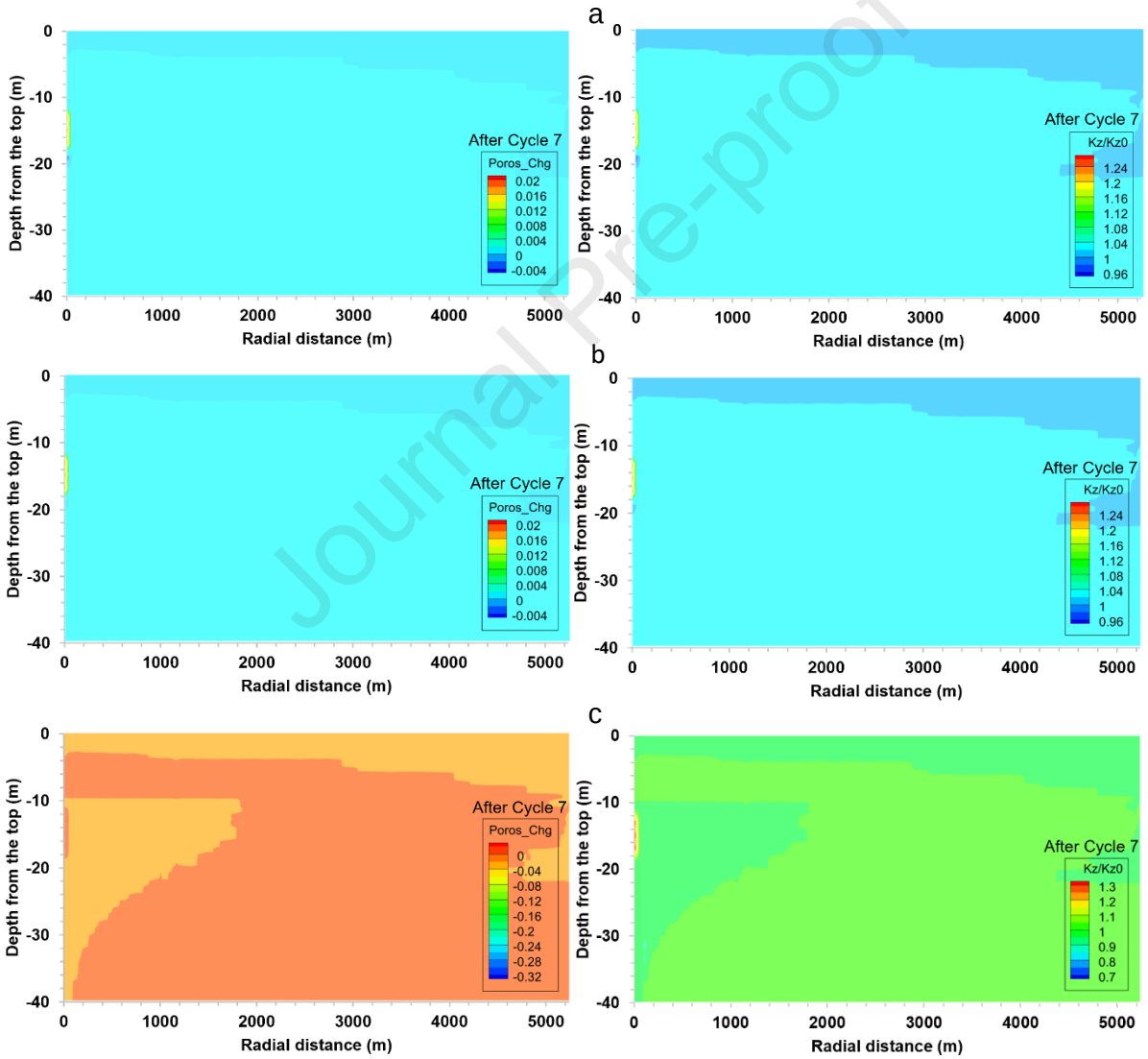

Figure 11: Porosity changes and permeability ratios for (a) CO_2 alone (b) CO_2-H_2S (c) CO_2-SO_2 injection cases in the formations after seven (7) cyclic injection-withdrawal processes.

After seven (7) cycles of CO_2 injection and withdrawal, for the CO_2 alone case, the maximum increase in porosity is 0.19% and 5.98% (corresponding to permeability increase of 0.59% and 26.70%) in the shale caprock and sandstone reservoir, respectively; while the maximum decrease in porosity is 0.03% and 1.56% (corresponding to permeability decrease of 0.10% and 6.12%) in the caprock and reservoir, respectively (Table 11). Similarly, for the CO_2-H_2S co-injection case, the maximum increase in porosity is 0.21% and 5.97% (corresponding to permeability increase of 0.66% and 26.68%) in the shale caprock and sandstone reservoir, respectively; while the maximum decrease in porosity is 0.03% and 1.54% (corresponding to permeability decrease of 0.10% and 6.06%) in the caprock and reservoir, respectively. In the case of CO_2-SO_2 co-injection, the maximum increase in porosity is 0.13% and 7.86% (corresponding to permeability increase of 0.40% and 36.29%) in the shale caprock and sandstone reservoir, respectively; while the maximum decrease in porosity is 0.3% and 4.42% (corresponding to permeability decrease of 0.92% and 16.54%) in the caprock and reservoir, respectively. For the CO_2-SO_2 co-injection case, the significant increase in porosity and permeability at the perforations in the production zone can be attributed to the severe dissolution of calcite, albite, chlorite, k-feldspar, and kaolinite minerals in that region, while the significant decrease in porosity and permeability in other regions of the sandstone reservoir contacted by SO_2 can be attributed mainly to the precipitation of anhydrite. These results are consistent with the results of some scholars (Bolourinejad and Herber, 2014; Pearce et al., 2016; Aminu et al., 2018), although they investigated the non-cyclic technique of CO_2 geosequestration. However, in the studies conducted by Bolourinejad and Herber (2014) and Aminu et al. (2018), porosity and permeability decreased in the reservoir during CO_2-H_2S co-injection. This result is different in the present study, as only a small amount of pyrite precipitated due to the low concentration of Fe^{2+} in the formation.

Table 11: Changes in porosity and permeability of the formations after seven (7) cycles of CO_2 injection and withdrawal.

Formation type	Petrophysics	After Cycle 7		
		CO_2	CO_2-H_2S	CO_2-SO_2
Shale caprock	Percentage change in porosity	-0.03 - 0.19	-0.03 - 0.21	-0.30 - 0.13
	Percentage change in permeability	-0.10 - 0.59	-0.10 - 0.66	-0.92 - 0.40
Sandstone reservoir	Percentage change in porosity	-1.56 - 5.98	-1.54 - 5.97	-4.42 - 7.86
	Percentage change in permeability	-6.12 - 26.70	-6.06 - 26.68	-16.54 - 36.29

4.2 Impact of impurities on the brittleness index of the sandstone reservoir and shale caprock during CO_2 geosequestration

The brittleness of sandstone and shale formations was evaluated at temperature and pressure conditions of 40^0C and 100 bar, respectively. The brittleness index of the rocks, considering the relative level of brittleness of brittle minerals as well as the simple sum of the fraction of brittle minerals is presented in Table 12 and Table 13. Table 12 shows the brittleness index of the rocks where the same molar volume of minerals are assumed to simplify the mineralogical brittleness index equations (equivalent to brittleness index without incorporating molar volume of minerals), while Table 13 shows the brittleness index of the rocks where the molar volumes of each mineral that makes up the rock are substituted in the mineralogical brittleness index equations (equivalent to brittleness index incorporating molar volume of minerals). So, Table 12 and Table 13 show that the initial brittleness index of the sandstone reservoir is significantly higher than that of the shale caprock. The relatively higher brittleness of sandstone formation before CO_2 sequestration is due to the high amount of the initial quartz and feldspar minerals, and some amount of calcite.

During CO_2 geosequestration, supercritical CO_2 (with or without impurities) was injected and withdrawn in cycles (up to seven cycles) for 87.5 years. SO_2 (or H_2S) gas hardly contacted the shale caprock up to 2-4 m vertical thickness from the reservoir (very low mole fraction, as higher concentration of SO_2 or H_2S is in the reservoir due to preferential dissolution of SO_2 (or H_2S) gas in the formation water. Thus, the brittleness of the shale caprock is largely dependent on the

reaction of CO_2 with the rock minerals. Hence, the brittleness of the shale caprock for all the injection cases decreased slightly during the period of CO_2 geosequestration.

Table 12: Brittleness index of the formations before and after the first and seventh cycles of CO_2 injection and withdrawal (eliminating molar volume).

Formation type	Brittleness index	Before sequestration, t=0			After cycle 1			After cycle 7		
		CO_2	CO_2-H_2S	CO_2-SO_2	CO_2	CO_2-H_2S	CO_2-SO_2	CO_2	CO_2-H_2S	CO_2-SO_2
Shale caprock	BI_{bm}	0.0377	0.0377	0.0377	0.0377	0.0377	0.0376-0.0377	0.0375-0.0377	0.0375-0.0377	0.0373-0.0377
	BI_{min}	0.0674	0.0674	0.0674	0.0673-0.0674	0.0673-0.0674	0.0673-0.0674	0.0671-0.0674	0.0671-0.0674	0.0666-0.0674
Sandstone Reservoir	BI_{bm}	0.4593	0.4593	0.4593	0.4585-0.4594	0.4585-0.4594	0.3457-0.4593	0.4582-0.4594	0.4582-0.4594	0.4433-0.4593
	BI_{min}	0.8642	0.8642	0.8642	0.8622-0.8644	0.8622-0.8644	0.6499-0.8642	0.8616-0.8645	0.8615-0.8645	0.8334-0.8642

Applying the brittleness index equations developed in the present study (and assuming all the minerals have the same molar volume and eliminating the molar volume parameter), the initial brittleness index (considering the relative level of brittleness of brittle minerals, BI_{bm}) of the shale caprock is 0.0377 (corresponding to brittleness index of 0.0674 using the simple sum of the fraction of brittle minerals, BI_{min}), while the initial brittleness index (BI_{bm}) of the sandstone reservoir is 0.4593 (BI_{min} =0.8642).

In this study, the brittleness index of the rocks was evaluated mainly by considering the relative level of brittleness of brittle minerals, using BI_{bm}. For the CO_2 alone and CO_2-H_2S co-injection cases, after the first cycle of gas injection and withdrawal, the brittleness index of the shale caprock remained 0.0377 (BI_{min} = 0.0673-0.0674). At the perforations in the production zone, the brittleness index (BI_{bm}) decreased from 0.4593 to 0.4585, representing a slight change in the brittleness index. A slight increase in brittleness index from 0.4593 to 0.4594 was observed at the vertical distance up to about 0-2 m reservoir thickness below the lower production perforation layer and less than 2 m lateral distance. The slight increase in the brittleness index might be attributed to the high amount of calcite dissolution close to the production perforations due to

severe erosion of the calcite mineral as CO_2 is produced in the production zone. Hence, some fraction of the calcite (brittle mineral) is deposited at the layers slightly below the production zone. In the CO_2-SO_2 co-injection case, after the first cycle of gas injection and withdrawal, the brittleness index of the shale caprock decreased slightly to about 0.0376 at the caprock layer contacted by SO_2. At the top two production perforations the brittleness index of the reservoir is 0.4586 and at the lowest production perforation the brittleness index is 0.3457, corresponding to significantly low porosity as all calcite minerals dissolved and precipitated large amount of anhydrite in that region as that region of the perforation interval has dissolved SO_2; while notable decrease in brittleness index down to 0.4499 was observed in other areas of the reservoir contacted by SO_2. However, at the perforations and regions in the reservoir [vertically and horizontally] close to the well perforations, the brittleness index might not be accurate for all the cycles of fluid injection and withdrawal, as the dissolved minerals in those regions or minerals that are deposited below the perforation interval close to the well are mainly unconsolidated materials (wellbore instability and fines deposition). Therefore, brittleness index evaluation based on the mineralogical composition from the numerical simulation would be more accurate farther away from the perforations (vertically and horizontally).

In the CO_2 alone and CO_2-H_2S co-injection cases, after the seventh cycle of gas injection and withdrawal, the brittleness index of the shale caprock decreased to about 0.0375. At the perforations in the production zone, the brittleness index is between 0.4582 and 0.4584, representing a negligible change in brittleness index after 75 years of CO_2 geosequestration (from the end of the first gas injection-withdrawal cycle). A slight increase in brittleness index up to 0.4594 (the same after the first cycle) was observed at the vertical distance up to about 0-4 m reservoir thickness and less than 2 m lateral distance below the lower production perforation layer. In the CO_2-SO_2 co-injection case, after the seventh cycle of gas injection and withdrawal, the brittleness index of the shale caprock decreased to about 0.0373 at the caprock layer contacted

by SO_2. At the production perforations, the brittleness index of the reservoir is 0.4588 (slightly higher than the first cycle), representing a negligible change in the brittleness index. However, a significant decrease in the brittleness index to about 0.4433 was observed in other areas of the reservoir contacted by SO_2.

Table 13 shows that incorporating the different molar volumes corresponding to each mineral in the rock (which converts the volume fraction of the minerals to the actual weight fraction of the minerals and is expected to be more accurate for estimating the brittleness index of rocks if the actual molar volumes of the minerals are incorporated) gives a higher brittleness index compared to when the molar volume parameter is eliminated from the brittleness index equation.

Table 13: Brittleness index of the formations before and after the first and seventh cycles of CO_2 injection and withdrawal (with molar volume).

Formation type	Brittleness index	Before sequestration, t=0			After cycle 1			After cycle 7		
		CO_2	CO_2-H_2S	CO_2-SO_2	CO_2	CO_2-H_2S	CO_2-SO_2	CO_2	CO_2-H_2S	CO_2-SO_2
Shale caprock	BI_{bm}	0.1073	0.1073	0.1073	0.1072-0.1073	0.1072-0.1073	0.1071-0.1073	0.1071-0.1073	0.1071-0.1073	0.1063-0.1073
	BI_{min}	0.1653	0.1653	0.1653	0.1651-0.1653	0.1651-0.1653	0.1649-0.1653	0.1649-0.1652	0.1649-0.1652	0.1633-0.1652
Sandstone Reservoir	BI_{bm}	0.5892	0.5892	0.5892	0.5887-0.5917	0.5887-0.5917	0.3672-0.5919	0.5885-0.5917	0.5885-0.5917	0.5575-0.5933
	BI_{min}	0.9307	0.9307	0.9307	0.9310-0.9285	0.9311-0.9285	0.5760-0.9307	0.9312-0.9280	0.9312-0.9280	0.8749-0.9307

Applying the brittleness index equations developed in the present study (and incorporating the different molar volume corresponding to each mineral in the rock), the initial brittleness index (considering the relative level of brittleness of brittle minerals, BI_{bm}) of the shale caprock is 0.1073 (corresponding to brittleness index of 0.1653 using the simple sum of the fraction of brittle minerals, BI_{min}), while the initial brittleness index (BI_{bm}) of the sandstone reservoir is 0.5892 (BI_{min} =0.9307). The change in brittleness index in the shale caprock is similar to what is observed when the molar volume parameter is eliminated from the equation. After seven cycles of CO_2 injection and withdrawal, the brittleness index decreased to about 0.1071 (BI_{min} = 0.1649) for the CO_2 alone

and CO_2-H_2S cases and decreased to about 0.1063 (BI_{min} = 0.1633) for the CO_2-SO_2 case. The percentage decrease in brittleness index (BI_{bm}) in the sandstone reservoir and shale caprock after seven cycles of injection and withdrawal for the CO_2-SO_2 case is 5.38% and 0.93%, respectively. The change in the brittleness index of the shale caprock, as well as the change in its porosity and permeability, during CO_2 geosequestration is negligible for all the cases considered. Therefore, the integrity of the caprock is maintained during cyclic CO_2 geosequestration. Overall, the decrease in brittleness of the shale caprock is consistent with the results of Lyu et al. (2018), although they adopted a non-cyclic technique of CO_2 sequestration. Lyu et al. (2018) applied the energy-balance method together with the Weibull distribution-based constitutive model to calculate the brittleness values of shale rock samples with or without [CO_2-brine] soaking conditions. They found that CO_2-brine-shale rock interactions decrease the brittleness values of the shale rock as well as its peak axial strength and Young's modulus.

Furthermore, the change in brittleness index in the sandstone reservoir is similar to what is observed when the molar volume parameter is eliminated from the equation, except at the perforations and regions in the reservoir [vertically and horizontally] close to the well perforations where the brittleness index by the simple sum of the fraction of brittle minerals did not correspond to the brittleness index by the relative level of brittleness of brittle minerals. For all the geosequestration cases (with or without impurities), BI_{min} decreased at the perforations, while BI_{bm} increased at the perforations. For the CO_2 alone and CO_2-H_2S cases, in the regions where it appears that minerals are deposited or precipitated minerals are unconsolidated (a few layers below the perforation interval and close to the well), BI_{min} increased, while BI_{bm} decreased, except for the CO_2-SO_2 case where both BI_{min} and BI_{bm} decreased mainly due to anhydrite precipitation. So, mineralogical brittleness index models might not be accurate at the perforations and regions in the reservoir [vertically and horizontally] close to the well perforations. Therefore, XRD analysis and mechanical tests on the change in the mineralogical and geomechanical properties of

sandstone rock samples and their fracture behaviour upon treatment with pure CO_2 or CO_2 mixture would be required to evaluate the correlation between the mineralogical brittleness index and mechanical brittleness index of the rock samples.

To quantify the reliable change between the brittleness index of rocks for the CO_2 alone and CO_2-SO_2 co-injection cases, the reliable change index was computed using brittleness index results (assuming all the minerals have the same molar volume and eliminating the molar volume parameter) from the CO_2 alone and CO_2-SO_2 co-injection cases at 87.5 years. The first column contains the brittleness index for the CO_2 alone case, while the second column contains the brittleness index of rocks for the CO_2-SO_2 co-injection case (a total of 1120 rows or observations). The Pearson's correlation coefficient (reliability coefficient, r) is 0.999747 (representing excellent reliability of the brittleness index), and the calculated standard deviation (σ) of the distribution of the brittleness index for the CO_2 alone case is 0.220965. Therefore, the reliable change index (with 95% confidence) is 0.009745. Hence, the absolute change in brittleness index between the CO_2 alone case and the CO_2-SO_2 co-injection case greater than 0.009745 Is considered significant. Therefore, in the present study, the change in the brittleness index of the sandstone reservoir for the CO_2-SO_2 co-injection case is significant.

The brittleness index calculated in this study based on the results from the numerical simulation for the CO_2 alone and CO_2-SO_2 co-injection cases were validated using an existing brittleness index model (BI_{BMod}) that utilizes the weight fraction of brittle minerals and considers relative bulk modulus of brittle minerals (Kang et al., 2020), and brittleness index model (BI_4) that considers the simple sum of weight fraction of brittle minerals, using the experimental data published by Mavhengere et al. (2022). The estimated brittleness index using the existing models is shown in Table 14. The existing models applied to the experimental data and the model adopted in the present study (based on the molecular weight, molar volume, and volume fraction of minerals) account for the significant change in the brittleness of the sandstone reservoir when SO_2 is co-

injected with CO_2. With pure CO_2, the change in the brittleness index of both ZC and ZG is negligible but changes significantly with the CO_2-SO_2 mixture.

Table 14: Brittleness index of ZC and ZG rock samples.

Sample	BI_4	BI_{BMod}
ZC untreated	0.93	0.68
ZC CO_2 treated	0.92	0.69
ZC CO_2-SO_2 treated	0.79	0.63
ZG untreated	0.76	0.52
ZG CO_2 treated	0.79	0.52
ZG CO_2-SO_2 treated	0.88	0.60

The alteration in the mineral phases of the ZC rock sample is similar to the sandstone reservoir in the present study, as the CO_2-SO_2 mixture resulted in a decrease in brittleness index of the rock; therefore, ZC sandstone was used to validate the mathematical model in the present study. Unlike ZC, for ZG, smectite (clay mineral) and stilbite dissolution were observed, while plagioclase and calcite precipitated, thereby inhibiting the precipitation of gypsum and increasing the brittleness index in the CO_2-SO_2 mixture case. The difference in the chemical reaction in the ZC and ZG sandstones is due to their mineralogical composition. For example, the ZG rock sample does not have calcite, pyrite, and diopside as primary minerals; whereas those are some of the primary minerals in ZC rock sample. Hence, only gypsum precipitated as a secondary mineral in ZC rock sample, while calcite precipitated as a secondary mineral in the ZG rock sample. Therefore, the impact of contaminants on the brittleness index of rocks depends on their (rocks') mineralogical composition. Furthermore, although the samples (sandstone samples from Zululand Basin) were held in the reactors in the CO_2 and gas mixture only for 2 months, this analysis confirms that the change in the brittleness index of rocks during the storage of pure CO_2 is negligible compared to how much CO_2-SO_2 mixture alters the brittleness of rocks.

However, sufficient laboratory experiments would be required to treat sandstone rock samples with CO_2-brine or CO_2-brine with gas impurities, followed by detailed XRD analyses and mechanical tests of the samples, to ascertain the change in their mineralogical and

geomechanical properties as well as the change in their fracture behaviour. These experiments and tests could also be extended to different shale and carbonate rocks.

5. Conclusions and Recommendations

5.1 Conclusions

In this study, a 2-D reactive transport model was developed for a cyclic approach of CO_2 geosequestration in a sandstone reservoir overlain by shale caprock. Furthermore, mathematical models were applied to evaluate the mineralogical brittleness index of the formations before and after CO_2 sequestration (with or without SO_2 or H_2S). Based on the key findings in this study, the conclusions are summarized as follows:

1. The preferential dissolution of SO_2 or H_2S gas into formation water (compared with CO_2 gas) leads to the delayed breakthrough of SO_2 or H_2S gas, and the separation between CO_2 and SO_2/H_2S gases at the moving front. In both co-injection cases, more SO_2/H_2S contains in the interior of the gas plume (during the CO_2 co-injection period, the mole fraction of SO_2/H_2S gas diminishes gradually from the injection well or perforation interval, laterally and upward as the CO_2 gas moves).
2. The total dissolved carbon (TDC) for all the geosequestration cases is nearly the same. This could be attributed to the convective mixing of the CO_2 (with or without H_2S/SO_2) with the formation water during the gas (supercritical fluid) withdrawal process, as additional pressure to produce the gas through the perforations in the production zone comes from the formation water. Thus, residually trapped CO_2 might have reconnected with the injected CO_2 in subsequent injection cycles, and water in rock pores containing dissolved H_2S or SO_2 might be flooded with water from different zones in the reservoir, enabling more CO_2 to be dissolved and resulting in a similar TDC for all the injection cases.
3. In all the injection cases, the porosity and permeability of the reservoir at the perforations in the production zone increased due to the severe dissolution of calcite and dissolution of some

of the primary minerals, creating more flow paths for the gas production. The porosity and permeability of the sandstone reservoir decreased in a few layers (and a small lateral distance in the reservoir) directly below the perforation interval in the production zone for all the injection cases. This decrease in porosity and permeability could be attributed to the deposition of dissolved (or eroded) minerals (especially calcite) or fines from the production zone in those layers. In other regions in the reservoir, the porosity and permeability increased for the CO_2 alone and CO_2-H_2S co-injection cases and decreased for the CO_2-SO_2 co-injection case.

4. The brittleness index of the sandstone reservoir and shale caprock decreased for all the injection cases, except at the perforations and regions in the reservoir [vertically and horizontally] close to the well perforations where the brittleness index models cannot account for accurately as the minerals in that region might constitute unconsolidated materials. A significant change (or decrease) in the brittleness index of the formations was observed only in the CO_2-SO_2 co-injection case due to a significant amount of anhydrite precipitation. The change in brittleness index in the formations for the CO_2 alone and CO_2-H_2S co-injection cases is negligible. Also, the change in brittleness index of the shale caprock, as well as its change in porosity and permeability during the cyclic CO_2 geosequestration is negligible. Therefore, the integrity of the caprock is maintained during CO_2 geosequestration (with or without the addition of small amount of H_2S or SO_2).

5.2 Recommendations for future study

1. Future studies should consider performing experiments to determine changes in the mechanical strengths (compressive and tensile strengths) and fracture behaviour of rocks subjected to cyclic injection and withdrawal, and their corresponding changes in the mechanical brittleness index of the rocks during CO_2 co-injection with H_2S or SO_2 gas.

2. Future studies should perform numerical simulations of cyclic injection and withdrawal over thousands of years and determine the impact of mineral trapping of CO_2, with solubility and residual trapping mechanisms, on the brittleness of rocks.
3. Further studies should be conducted to investigate fines migration from the reservoir to the well or tubing string during cyclic injection and withdrawal of CO_2.

Author credit statement

Efenwengbe Nicholas Aminaho: Conceptualization, Investigation, Methodology, Validation, Analyses, and Writing. **Mamdud Hossain:** Supervisor. **Nadimul Haque Faisal:** Supervisor. **Reza Sanaee:** Supervisor.

Declaration of competing interest

The authors declare that they have no known competing financial interests or personal relationships that could have appeared to influence the work reported in this paper.

Acknowledgements

The authors would like to acknowledge the flexible funding and partnership offered by the UK Carbon Capture and Storage Research Community (UKCCSRC). This project was jointly funded by Robert Gordon University (Aberdeen) and UKCCSRC.

REFERENCES

Abedini, A. and Torabi, F. (2014). On the CO_2 storage potential of cyclic CO_2 injection process for enhanced oil recovery. *Fuel,* 124, pp. 14-27.

AL-Ameri, W.A., Abdulraheem, A. and Mahmoud, M. (2016). Long-term effects of CO_2 sequestration on rock mechanical properties. *Journal of Energy Resources Technology*, 138, pp. 1-9.

Aminaho, E.N. and Hossain, M. (2023). Caprock integrity evaluation for geosequestration of CO_2 in low-temperature reservoirs. Aberdeen: Robert Gordon University. https://rgu-repository.worktribe.com/output/2072081

Aminu, M.D., Nabavi, S.A. and Manovic, V. (2018) CO_2-brine-rock interactions: The effect of impurities on grain size distribution and reservoir permeability. *International Journal of Greenhouse Gas Control, 7*8, pp. 168-176.

Bachu, S. (2002). Sequestration of CO_2 in geological media in response to climate change: road map for site selection using the transform of the geological space into the CO_2 phase space. *Energy Conversion and Management,* 43, pp. 87-102.

Badrouchi, N., Pu, H., Smith, S., Yu, Y. and Badrouchi, F. (2022). Experimental investigation of CO2 injection side effects on reservoir properties in ultra tight formations. *Journal of Petroleum Science and Engineering,* 215, pp. 1-9.

Blampied, N.M. (2016). Reliable change & the reliable change index in the context of evidence-based practice: A tutorial review. Paper presented at the NZPsS Conference, Wellington, 2-4 September 2016.

Bolourinejad, P. and Herber, R. (2014) Experimental and modelling study of storage of CO_2 and impurities in a depleted gas field in northeast Netherlands. *Energy Procedia,* 63, pp. 2811-2820.

Deer, D.A., Howie, R.A. and Zussman, J. (1966). *An introduction to the rock forming minerals.* Essex: Longman Scientific & Technical.

Edlmann, K., Hinchliffe, S., Heinemann, N., Johnson, G., Ennis-King, J. and McDermott, C.I. (2019). Cyclic CO_2-H_2O injection and residual trapping: Implications for CO_2 injection efficiency and storage security. *International Journal of Greenhouse Gas Control,* 80, pp. 1-9.

Elwegaa, K., Emadi, H., Soliman, M., Gamadi, T. and Elsharafi, M. (2019). Improving oil recovery from shale oil reservoirs using cyclic cold carbon dioxide injection – An experimental study. *Fuel,* 254, 115586.

Ezema, I.C., Edelugo, S.O., Menon, A.R.R. and Omah, A.D. (2015). A Comparative Prediction of the Tensile Properties of Sisal Fiber Reinforced Epoxy Composite Using Volume Fraction and Mass Fraction Models. *Journal of Metallurgical and Materials Engineering Research*, 1 (2), pp. 9-18.

Fatima, S., Khan, H.M.M., Tariq, Z., Abdalla, M. and Mahmoud, M. (2021). An Experimental and Simulation Study of CO_2 Sequestration in Underground Formations: Impact on Geomechanical and Petrophysical Properties. Paper (SPE-204726-MS) presented at the SPE Middle East Oil & Gas Show and Conference, November 28–December 1, 2021.

Fjaer, E., Holt, R.M., Horsrud, P., Raaen, A.M. and Risnes, R. (2008). *Petroleum Related Rock Mechanics*. Developments in Petroleum Science. Vol 53. 2nd ed. Amsterdam: Elsevier.

Gong, Q.M. and Zhao, J. (2007). Influence of rock brittleness on TBM penetration rate in Singapore granite. *Tunn. Undergr. Space Technol*, 22 (3), pp. 317–324.

Guo, L., Jiang, Z. and Liang, C. (2016). Mineralogy and Shale Gas Potential of Lower Silurian Organic-Rich Shale at the Southeastern Margin of Sichuan Basin, South China. *Oil Shale*, 33 (1), pp. 1–17.

Hedayati, M., Wigston, A., Wolf, J.L., Rebscher, D. and Niemi, A. (2018). Impacts of SO_2 gas impurity within a CO_2 stream on reservoir rock of a CCS pilot site: experimental and modelling approach. *International Journal of Greenhouse Gas Control*, 70, pp. 32–44. DOI: https://doi.org/10.1016/j.ijggc.2018.01.003

Herring, A.L., Anderson, L. and Wildenschild, D. (2016). Enhancing residual trapping of supercritical CO_2 via cyclic injections. *Geophysical Research Letters*, 43 (18), pp. 9677-9685.

Hou, B., Zeng, Y., Fan, M. and Li, D. (2018). Brittleness Evaluation of Shale Based on the Brazilian Splitting Test. *Geofluids,* 2018, pp. 1-11.

Hucka, V. and Das, B. (1974). Brittleness Determination of Rocks by Different Methods. *Int. J. Rock Mech. Min. Sci. & Geomech*, 11, pp. 389-392.

Jin, X., Shah, S.N., Roegiers, J.-C. and Zhang, B. (2015). An Integrated Petrophysics and Geomechanics Approach for Fracability Evaluation in Shale Reservoirs. *SPE Journal,* 20 (3), pp. 518-526.

Kang, Y., Shang, C., Zhou, H., Huang, Y., Zhao, Q. Deng, Z., Wang, H. and Ma, Y.Z. (2020). Mineralogical brittleness index as a function of weighting brittle minerals—from laboratory tests to case study. *Journal of Natural Gas Science and Engineering,* 77, pp. 1-9.

Ke, Q., Li, C., Yao, W., Fan, Y., Zhan, H., Li., B. and Zhang, X. (2023). Comparative characterization of sandstone microstructure affected by cyclic wetting-drying process. *International Journal of Rock Mechanics & Mining Sciences*, 170, pp. 1-10.

Kim, C., Kim, J., Joo, S., Bu, Y., Liu, M., Cho, J. and Kim, G. (2018). Efficient CO_2 utilization via a hybrid Na-CO_2 system based on CO_2 dissolution. *iScience, 9, pp. 278 – 285.*

Klokov, A., Treviño, R.H. and Meckel, T.A. (2017) Diffraction imaging for seal evaluation using ultra high resolution 3D seismic data. *Marine and Petroleum Geology*, 82, pp. 85-96.

Koomson, S., Park, S., Kim, W., No, C., Lee, C., Choi, H. and Lee, C.-G. (2023). Electrochemical hydrogen production using captured CO2 in alkaline solution. *International Journal of Electrochemical Science,* 18, pp. 1-7.

Lasaga, A.C., Soler, J.M., Ganor, J., Burch, T.E. and Nagy, K.L. (1994). Chemical weathering rate laws and global geochemical cycles. *Geochimica et Cosmochimica Acta*, 58, pp. 2361-2386.

Li, C., Zhang, F., Lyu, C., Hao, J., Song, J. and Zhang, S. (2016). Effects of H_2S injection on the CO_2-brine-sandstone interaction under 21 MPa and 70 °C. *Marine Pollution Bulletin,* 106, pp. 17–24.

Li, D., Saraji, S., Jiao, Z. and Zhang, Y. (2021). CO_2 injection strategies for enhanced oil recovery and geological sequestration in a tight reservoir: An experimental study. *Fuel,* 284, 1-11.

Li, G., Jin, Z., Li, X., Liu, K., Yang, W., Qiao, M., Zhou, T. and Sun, X. (2023). Experimental study on mechanical properties and fracture characteristics of shale layered samples with different mineral components under cyclic loading. *Marine and Petroleum Geology,* 150, pp. 1-14.

Li, H. (2022). Research progress on evaluation methods and factors influencing shale brittleness: A review. Energy Reports, 8, pp. 4344–4358.

Liu, Y., Ma, T., Wu, H. and Chen, P. (2020) Investigation on mechanical behaviors of shale cap rock for geological energy storage by linking macroscopic to mesoscopic failures. *Journal of Energy Storage*, 29, pp. 1-15.

López-Rendón, R. and Alejandre, J. (2008). Molecular dynamics simulations of the solubility of H_2S and CO_2 in water. *J. Mex. Chem. Soc*., 52 (1), pp. 88-92.

Lysyy, M., Liu, N., Solstad, C.M., Fernø, M.A. and Ersland, G. (2023). Microfluidic hydrogen storage capacity and residual trapping during cyclic injections: Implications for underground storage. *International Journal of Hydrogen Energy.* https://doi.org/10.1016/j.ijhydene.2023.04.253

Lyu, Q., Long, X., Ranjith, P.G., Tan, J., Kang, Y. and Luo, W. (2018). A Damage Constitutive Model for the Effects of CO_2-Brine-Rock Interactions on the Brittleness of a Low-Clay Shale. *Geofluids*, pp. 1-14.

Ma, X., Yang, G., Li, X., Yu, Y. and Dong, J. (2019). Geochemical modelling of changes in caprock permeability caused by CO_2–brine–rock interactions under the diffusion mechanism. *Oil & Gas Science and Technology - Rev. IFP Energies Nouvelles*, 74 (83), pp. 1-13.

Marini, L. ed. (2007). "The Product Solid Phases" in Geological Sequestration of Carbon Dioxide: Thermodynamics, Kinetics, and Reaction Path Modelling. *Developments in Geochemistry*, 11, pp. 79-167. https://doi.org/10.1016/S0921-3198(06)80025-6

Mavhengere, P., Wagner, N. and Malumbazo, N. (2022). Influences of SO_2 contamination in long term supercritical CO_2 treatment on the physical and structural characteristics of the Zululand Basin caprock and reservoir core samples. *Journal of Petroleum Science and Engineering*, 215, pp. 1-15.

Meng, F., Zhou, H., Zhang, C., Xu, R. and Lu, J. (2015). Evaluation Methodology of Brittleness of Rock Based on Post-Peak Stress–Strain Curves. *Rock Mech Rock Eng*, 48, pp. 1787–1805.

Miri, R., Aagaard, P. and Hellevang, H. (2014). Examination of CO_2-SO_2 solubility in water by SAFT1: Implications for CO_2 transport and storage. *J. Phys. Chem. B*, 118, pp. 10214-10223.

Panfilov, M. (2016). 'Underground and pipeline hydrogen storage', in B. Ram et al. (eds) Compendium of Hydrogen Engergy. Woodhead Publishing, 2, pp. 91-115. https://doi.org/10.1016/B978-1-78242-362-1.00004-3

Pearce, J.K., Dawson, G.K.W, Law, A.C.K., Biddle, D. and Golding, S.D. (2016) Reactivity of micas and cap-rock in wet supercritical CO_2 with SO_2 and O_2 at CO_2 storage conditions. *Applied Geochemistry,* 72, pp. 59-76.

Pearce, J.K., Kirste, D.M., Dawson, G.K.W., Rudolph, V. and Golding, S.D. (2019) Geochemical modelling of experimental O_2–SO_2–CO_2 reactions of reservoir, cap-rock, and overlying cores. *Applied Geochemistry,* 109, pp. 1-19.

Pruess, K. (2004). The TOUGH Codes - A family of simulation tools for multiphase flow and transport processes in permeable media. *Vadose Zone Journal*, 3, pp. 738-746.

Reeves, S. (2001). Geologic sequestration of CO_2 in deep, unmineable coalbeds: an integrated research and commercial-scale field demonstration project. First National Carbon Sequestration Conference, U.S.DOE/NETL, pp. 1-12.

Robie, R.A., Bethke, P.M. and Beardsley, K.M. (1967). *Selected x-ray crystallographic data molar volumes, and densities of minerals and related substances*. Washington: United States Government Printing Office, pp. 42-72.

Sánchez-Díaz, Á (2017). MefCO_2 – Synthesis of methanol from captured carbon dioxide using surplus electricity (EU-H2020). *Impact,* 2017 (5), pp. 6-8.

Schifflechner, C., Wieland, C. and Spliethoff, H. (2022). CO_2 plume geothermal (CPG) systems for combined heat and power production: an evaluation of various plant configurations. *Journal of Thermal Science*, 31(5), pp. 1266-1278.

Shafiq, M.U., Mahmud, H.K.B., Wang, L., Abid, K. and Gishkori, S.N. (2022). Comparative elemental, mineral and microscopic investigation of sandstone matrix acidizing at HPHT conditions. *Petroleum Research*, 7, pp. 448-458.

Shen, X., Kolluru, G.K., Yuan, S. and Kevil, C.G. (2015). 'Measurement of H_2S In Vivo and In Vitro by the Monobromobimane Method', in Cadenas, E. and Packer, L. (eds) Methods in Enzymology. Academic Press, 554, pp. 31-45. https://doi.org/10.1016/bs.mie.2014.11.039

SNC-Lavalin Inc. (2004). Impact of Impurities on CO_2 Capture, Transport and Storage. IEA Greenhouse Gas R&D Programme Report (No. PH4/32).

Sollai, S., Porcu, A., Tola, V., Ferrara, F. and Pettinau, A. (2023). Renewable methanol production from green hydrogen and captured CO_2: A techno-economic assessment. *Journal of CO_2 Utilization,* 68, pp. 1-12.

Su, E., Liang, Y., Chang, X., Zou, Q., Xu, M. and Sasmito, A.P. (2020). Effects of cyclic saturation of supercritical CO_2 on the pore structures and mechanical properties of bituminous coal: An experimental study. *Journal of CO_2 Utilization,* 40, pp. 1-12.

Su, E., Liang, Y. and Zou, Q. (2021). Structures and fractal characteristics of pores in long-flame coal after cyclical supercritical CO_2 treatment. *Fuel,* 286, pp. 1-12.

Sun, Y., Li, Q., Yang, D. and Liu, X. (2016). Laboratory core flooding experimental systems for CO_2 geosequestration: An updated review over the past decade. Journal of Rock Mechanics and Geotechnical Engineering, 8, pp. 113-126.

Totten, M.W., Hanan, M.A., Knight, D. and Borges, J. (2002). Characteristics of mixed-layer smectite/illite density separates during burial diagenesis. *American Mineralogist,* 87, pp. 1571-1579.

Wang, D., Li, J., Meng, W., Liao, Z., Yang, S., Hong, X., Zhou, H., Yang, Y. and Li, G. (2023). A near-zero carbon emission methanol production through CO_2 hydrogenation integrated with

renewable hydrogen: Process analysis, modification and evaluation. *Journal of Cleaner Production,* 412, pp. 1-15.

Wang, H., Zhang, L., Lei, H., Wang, Y., Liu, H., Li, X. and Su, X. (2021). Potential for uranium release under geologic CO_2 storage conditions: The impact of Fe(III). *International Journal of Greenhouse Gas Control,* 107, 103266. https://doi.org/10.1016/j.ijggc.2021.103266

Wang, J., Zhao, Y., An, Z. and Shabani, A. (2022). CO_2 storage in carbonate rocks: An experimental and geochemical modelling study. *Journal of Geochemical Exploration,* 234, pp. 1-14.

Wang, L., Zhang, Y., Liu, Y., Xie, H., Xu, Y. and Wei, J. (2020). SO_2 absorption in pure ionic liquids: Solubility and functionalization. *Journal of Hazardous Materials*, 392, 122504. https://doi.org/10.1016/j.jhazmat.2020.122504

Wei, X.C., Li, Q., Li, X.-Y., Sun, Y.-K. and Liu, X.H. (2015) Uncertainty analysis of impact indicators for the integrity of combined caprock during CO_2 geosequestration. *Engineering Geology*, 196, pp. 37–46.

Xu, J., Zhai, C., Ranjith, P.G., Sun, Y., Cong, Y., Zheng, Y., Tang, W. and Yang, W. (2021). Investigation of non-isothermal effect of cyclic carbon dioxide on the petrography of coals for coal mine methane recovery. *Fuel,* 290, pp. 1-12.

Xu, T., Sonnenthal, E., Spycher, N. and Pruess, K. (2006). TOUGHREACT: A simulation program for non-isothermal multiphase reactive geochemical transport in variably saturated geologic media. *Computer & Geosciences,* 32, pp. 145-165. https://doi.org/10.1016/j.cageo.2005.06.014

Xu, T., Sonnenthal, E., Spycher, N. and Zheng, L. (2014). TOUGHREACT V3.0-OMP Reference Manual: A Parallel Simulation Program for Non-Isothermal Multiphase Geochemical Reactive Transport.

Zhang, D., Ranjith, P.G. and Perera, M.S.A. (2016). The brittleness indices used in rock mechanics and their application in shale hydraulic fracturing: A review. *Journal of Petroleum Science and Engineering,* 143, pp. 158–170.

Zhang, W., Xu, T. and Li, Y. (2010). Modelling of fate and transport of co-injection of H_2S with CO_2 in deep saline formations. United States. DOI: https://www.osti.gov/servlets/purl/1007193

Zheng, L., Apps, J.A., Zhang, Y., Xu, T. and Birkholzer, J.T. (2009). On mobilization of lead and arsenic in groundwater in response to CO_2 leakage from deep geological storage. *Chemical Geology*, 268, (3-4), pp. 281-297.

Table 1: Bulk modulus of different brittle minerals (Fjaer et al., 2008).

Brittle mineral	Quartz	Feldspar	Calcite	Dolomite
Bulk modulus (GPa)	37.5	76	74	76-95

Table 2: Weighting coefficients of different brittle minerals (Kang et al., 2020).

Brittle mineral	Quartz	Feldspar	Calcite	Dolomite
Weighting coefficient	1	0.49	0.51	0.39-0.49/0.44

Table 3: Mesh generation of the model.

Rock formation	**Vertical mesh number**	**Mesh thickness (m)**
Shale caprock	6	2.0
Sandstone reservoir	14	2.0

Table 4: Hydrogeological parameters used in the simulation at formation temperature and pressure of 40^{0}C and 100 bar, respectively.

Parameters	**Formation**	
	Sandstone	**Shale caprock**
Porosity	0.34	0.07
Horizontal permeability (m^2)	2.264×10^{-13}	2.264×10^{-16}
Vertical permeability (m^2)	2.264×10^{-14}	2.264×10^{-17}
Pore compressibility (Pa^{-1})	2.10×10^{-9}	2.10×10^{-9}
Rock grain density (kg/m^3)	2600	2600
Formation heat conductivity (W/m ^{0}C)	2.51	2.51
Rock grain specific heat (J/kg ^{0}C)	920.0	920.0
Temperature (^{0}C)	40.0	40.0
Salinity (mass fraction)	0.06	0.06
Pressure (bar)	100	100
Initial gas saturation	0.00	0.00
CO_2 injection rate (kg/s)	20.0	-
CO_2 withdrawal rate (kg/s)	15.0	-
Relative permeability Liquid: Van Genuchten function $k_{rl} = \sqrt{S^*}\left\{1 - \left(1 - [S^*]^{1/m}\right)^m\right\}^2$ S_{lr}: residual water saturation m: exponent Gas: Corey $k_{rg} = (1 - \hat{S})^2(1 - \hat{S}^2)$ S_{gr}: residual gas saturation	$S^* = (S_l - S_{lr})/(1 - S_{lr})$ $S_{lr} = 0.30$ $m = 0.457$ $\hat{S} = (S_l - S_{lr})/(1 - S_{lr} - S_{gr})$ $S_{gr} = 0.05$	
Capillary pressure Van Genuchten function $P_{cap} = -P_0\left([S^*]^{-1/m} - 1\right)^{1-m}$ S_{lr}: residual water saturation m: exponent	$S^* = (S_l - S_{lr})/(1 - S_{lr})$ $S_{lr} = 0.03$ $m = 0.457$	
P_0: strength coefficient	19.61 kPa	19.61 kPa

Table 5: Initial volume fractions of the minerals and their molecular weight and molar volume.

Mineral name	Chemical formula	Molecular weight (g/mol)	Molar volume (cm^3/mol)	Sandstone formation (volume percent of solid)	Shale Caprock (volume percent of solid)
Illite	$K_{0.6}Mg_{0.25}Al_{1.8}(Al_{0.5}Si_{3.5}O_{10})(OH)_2$	383.899	138.900	2.80	65.30
Kaolinite	$Al_2Si_2O_5(OH)_4$	258.159	99.520	0.90	1.11
Smectite-Ca	$Ca_{0.145}Mg_{0.26}Al_{1.77}Si_{3.97}O_{10}(OH)_2$	365.394	140.536	0	6.96
Chlorite	$Mg_{2.5}Fe_{2.5}Al_2Si_3O_{10}(OH)_8$	634.648	210.260	2.70	6.40
Quartz	SiO_2	60.084	22.688	25.80	8.00
K-feldspar	$KAlSi_3O_8$	278.33	108.900	23.30	2.80
Albite	$NaAlSi_3O_8$	262.222	100.070	41.50	3.20
Calcite	$CaCO_3$	100.087	36.934	3.00	0.80
Pyrite	FeS_2	119.98	23.940	0	1.43
Dolomite	$CaMg(CO_3)_2$	184.401	64.341	0	0
Anhydrite	$CaSO_4$	136.142	45.940	0	4.00
Siderite	$FeCO_3$	115.856	146.800	0	0
Alunite	$KAl_3(OH)_6(SO_4)_2$	414.214	69.522	0	0
Ankerite	$CaMg_{0.3}Fe_{0.7}(CO_3)_2$	206.48	58.520	0	0
Dawsonite	$NaAlCO_3(OH)_2$	143.995	28.018	0	0
Magnesite	$MgCO_3$	84.314	29.378	0	0
Smectite-Na	$Na_{0.290}Mg_{0.26}Al_{1.77}Si_{3.97}O_{10}(OH)_2$	366.25	132.510	0	0
Hematite	Fe_2O_3	159.692	30.274	0	0
Anorthite	$CaAl_2Si_2O_8$	278.206	100.790	0	0
Muscovite	$KAl_2(AlSi_3O_{10})(F,OH)_2$	398.306	140.710	0	0
Oligoclase	$CaNa_4Al_6Si_{14}O_{40}$	1327.094	502.480	0	0

Table 6: Initial chemical composition of the formation water at formation conditions of 40^0C and 100 bar.

Component	Concentration (mol/kg H_2O)	
	Sandstone formation	Shale caprock
Ca^{2+}	4.7137E-01	4.8163E-01
Mg^{2+}	1.0038E-01	9.7547E-02
Na^{+}	2.5868E+00	2.6006E+00
K^{+}	2.8166E-03	3.3113E-03
Fe^{2+}	4.9784E-04	2.7904E-08
SiO_2 (aq)	2.9555E-03	1.3991E-03
HCO_3^{-}	2.1733E-03	1.2688E-04
SO_4^{2-}	3.6425E-03	1.7486E-02
AlO_2^{-}	1.3611E-11	6.1835E-11
Cl^{-}	3.7245E+00	3.7264E+00
pH	6.1989	7.3919

Table 7: List of parameters for calculating the kinetic rate of minerals.

Mineral name	Initial reactive surface area (cm^2/g)	Neutral mechanism		Acid mechanism			Base mechanism		
		K_{25} (mol/m^2s)	E_a (kJ/mol)	K_{25} (mol/m^2s)	E_a (kJ/mol)	$n(H^+)$	K_{25} (mol/m^2s)	E_a (kJ/mol)	$n(H^+)$
Calcite	Assumed in equilibrium								
Anhydrite	Assumed in equilibrium								
Quartz	9.8	1.0233E-14	87.7						
Kaolinite	151.63	6.9183E-14	22.2	4.8978E-12	65.90	0.777	8.9125E-18	17.90	-0.472
Illite	151.63	1.6596E-13	35.00	1.0471E-11	23.6	0.34	3.02E-17	58.9	-0.40
Pyrite	12.87	2.8184E-05	56.90 $n_{O2(aq)}$=0.5	3.02E-08	56.9	n_{H+}=-0.5 n_{Fe3+}=0.5			
K-feldspar	9.8	3.8905E-13	38.0	8.7096E-11	51.7	0.5	6.3096E-22	94.1	-0.823
Dolomite	9.8	2.9512E-08	52.20	6.4565E-04	36.1	0.5			
Siderite	9.8	1.2598E-09	62.76	6.4565E-04	36.1	0.5			
Ankerite	9.8	1.2598E-09	62.76	6.4565E-04	36.1	0.5			
Albite	9.8	2.7542E-13	69.80	6.9183E-11	65.0	0.457	2.5119E-16	71.0	-0.572
Muscovite	9.8	3.160E-13	58.6						
Hematite	12.87	2.5119E-15	66.2	4.0738E-10	66.2	1.0			
Chlorite	9.8	3.020E-13	88.0	7.7624E-12	88.0	0.5			
Oligoclase	9.8	1.4454E-13	69.8	2.1380E-11	65.0	0.457			
Magnesite	9.8	4.5709E-10	23.5	4.1687E-07	14.4	1.0			
Dawsonite	9.8	1.2598E-09	62.76	6.4565E-04	36.1	0.5			
Smectite-Na	151.63	1.6596E-13	35.0	1.0471E-11	23.6	0.34	3.0200E-17	58.9	-0.40
Smectite-Ca	151.63	1.6596E-13	35.0	1.0471E-11	23.6	0.34	3.0200E-17	58.9	-0.40
Alunite	9.8	1.0000E-12	57.78				1.0000E-12	7.5	-1.00
Anorthite	9.8	1.5000E-14	18.4						

Table 8: Three groups of simulations in this study.

Simulation groups	Injection scenarios	Formation	Formation salinity
1	CO_2 only	Sandstone and shale	0.06
2	CO_2 and H_2S	Sandstone and shale	0.06
3	CO_2 and SO_2	Sandstone and shale	0.06

Table 9: ZC and ZG core samples XRD results before and after $ScCO_2$-water and $ScCO_2$-SO_2-water treatment (Mavhengere et al., 2022).

Sample	Quartz (wt. %)	Plagioclase (wt. %)	Smectite (wt. %)	Calcite (wt. %)	Pyrite (wt. %)	Stilbite (wt. %)	Diopside (wt. %)	Gypsum (wt. %)	Orthoclase (wt. %)
ZC untreated	44.1	44.7	1.0	3.5	0.4	3.6	2.7	0.0	0.0
ZC CO_2 treated	47.5	42.5	2.5	1.7	0.4	2.7	2.8	0.0	0.0
ZC CO_2-SO_2 treated	49.1	28.6	11.8	0.0	0.8	4.9	2.3	2.5	0.0
ZG untreated	21.5	46.0	22.2	0.0	0.0	2.0	0.0	0.0	8.3
ZG CO_2 treated	22.3	50.5	16.3	2.9	0.0	4.8	0.0	0.0	3.2
ZG CO_2-SO_2 treated	26.1	53.4	12.1	2.3	0.0	0.0	0.0	0.0	6.2

Table 10: Porosity and permeability ratio of the formations after seven (7) cycles of CO_2 injection and withdrawal.

Formation type	Petrophysics	After Cycle 7		
		CO_2	CO_2-H_2S	CO_2-SO_2
Shale caprock	Porosity	0.06998-0.07013	0.06998-0.07015	0.06979-0.07009
	Permeability ratio	0.99904-1.00590	0.99903-1.00660	0.99078-1.00400
Sandstone reservoir	Porosity	0.33470-0.36032	0.33475-0.36031	0.32496-0.36672
	Permeability ratio	0.93881-1.26700	0.93943-1.26680	0.83462-1.36290

Table 11: Changes in porosity and permeability of the formations after seven (7) cycles of CO_2 injection and withdrawal.

Formation type	Petrophysics	After Cycle 7		
		CO_2	CO_2-H_2S	CO_2-SO_2
Shale caprock	Percentage change in porosity	-0.03 - 0.19	-0.03 - 0.21	-0.30 - 0.13
	Percentage change in permeability	-0.10 - 0.59	-0.10 - 0.66	-0.92 - 0.40
Sandstone reservoir	Percentage change in porosity	-1.56 - 5.98	-1.54 - 5.97	-4.42 - 7.86
	Percentage change in permeability	-6.12 - 26.70	-6.06 - 26.68	-16.54 - 36.29

Table 12: Brittleness index of the formations before and after the first and seventh cycles of CO_2 injection and withdrawal (eliminating molar volume).

Formation type	Brittleness index	Before sequestration, t=0			After cycle 1			After cycle 7		
		CO_2	CO_2-H_2S	CO_2-SO_2	CO_2	CO_2-H_2S	CO_2-SO_2	CO_2	CO_2-H_2S	CO_2-SO_2
Shale caprock	BI_{bm}	0.0377	0.0377	0.0377	0.0377	0.0377	0.0376-0.0377	0.0375-0.0377	0.0375-0.0377	0.0373-0.0377
	BI_{min}	0.0674	0.0674	0.0674	0.0673-0.0674	0.0673-0.0674	0.0673-0.0674	0.0671-0.0674	0.0671-0.0674	0.0666-0.0674
Sandstone Reservoir	BI_{bm}	0.4593	0.4593	0.4593	0.4585-0.4594	0.4585-0.4594	0.3457-0.4593	0.4582-0.4594	0.4582-0.4594	0.4433-0.4593
	BI_{min}	0.8642	0.8642	0.8642	0.8622-0.8644	0.8622-0.8644	0.6499-0.8642	0.8616-0.8645	0.8615-0.8645	0.8334-0.8642

Table 13: Brittleness index of the formations before and after the first and seventh cycles of CO_2 injection and withdrawal (with molar volume).

Formation type	Brittleness index	Before sequestration, t=0			After cycle 1			After cycle 7		
		CO_2	CO_2-H_2S	CO_2-SO_2	CO_2	CO_2-H_2S	CO_2-SO_2	CO_2	CO_2-H_2S	CO_2-SO_2
Shale caprock	BI_{bm}	0.1073	0.1073	0.1073	0.1072-0.1073	0.1072-0.1073	0.1071-0.1073	0.1071-0.1073	0.1071-0.1073	0.1063-0.1073
	BI_{min}	0.1653	0.1653	0.1653	0.1651-0.1653	0.1651-0.1653	0.1649-0.1653	0.1649-0.1652	0.1649-0.1652	0.1633-0.1652
Sandstone Reservoir	BI_{bm}	0.5892	0.5892	0.5892	0.5887-0.5917	0.5887-0.5917	0.3672-0.5919	0.5885-0.5917	0.5885-0.5917	0.5575-0.5933
	BI_{min}	0.9307	0.9307	0.9307	0.9310-0.9285	0.9311-0.9285	0.5760-0.9307	0.9312-0.9280	0.9312-0.9280	0.8749-0.9307

Table 14: Brittleness index of ZC and ZG rock samples.

Sample	BI_4	BI_{BMod}
ZC untreated	0.93	0.68
ZC CO_2 treated	0.92	0.69
ZC CO_2-SO_2 treated	0.79	0.63
ZG untreated	0.76	0.52
ZG CO_2 treated	0.79	0.52
ZG CO_2-SO_2 treated	0.88	0.60

HIGHLIGHTS

- SO_2 gas front is far behind that of CO_2 in the sandstone reservoir, compared to the H_2S case.
- The porosity of the reservoir decreases a few layers directly below the production zone.
- The brittleness of the shale caprock decreases slightly during CO_2 geosequestration.
- The decrease in brittleness of the sandstone reservoir is negligible except for CO_2-SO_2 case.
- Compared to H_2S, SO_2 significantly decreases the brittleness of the sandstone reservoir.

AUTHORS INFORMATION

Authors names: Efenwengbe Nicholas Aminaho[a], Mamdud Hossain[a], Nadimul Haque Faisal[a], and Reza Sanaee[a,b].

Authors affiliations:

a: Robert Gordon University, School of Engineering, Aberdeen, United Kingdom.
b: COWI

Author contact details:

Efenwengbe Nicholas Aminaho: aminahonicholas@gmail.com
Mamdud Hossain: m.hossain@rgu.ac.uk
Nadimul Haque Faisal: N.H.Faisal@rgu.ac.uk
Reza Sanaee: r.sanaee@rgu.ac.uk
rese@cowi.com

Corresponding author: Efenwengbe Nicholas Aminaho

Corresponding author email address: aminahonicholas@gmail.com

Author credit statement

Efenwengbe Nicholas Aminaho: Conceptualization, Investigation, Methodology, Validation, Analyses, and Writing. **Mamdud Hossain:** Supervision and Review. **Nadimul Haque Faisal:** Supervision. **Reza Sanaee:** Supervision.

Declaration of competing interest

The authors declare that they have no known competing financial interests or personal relationships that could have appeared to influence the work reported in this paper.

Acknowledgements

The authors would like to acknowledge the flexible funding and partnership offered by the UK Carbon Capture and Storage Research Community (UKCCSRC). The UKCCSRC is supported by the Engineering and Physical Sciences Research Council (ESPRC) as part of the UK Research and Innovation (UKRI) Energy Programme. This project is jointly funded by Robert Gordon University (Aberdeen) and UKCCSRC.